Supporting Information for

Sulfur Dioxide Sulfide (SSO_2): The Elusive Isovalent Analogue of Sulfur Trioxide (SO_3)

Mason McAnally[a,b§], Xilin Bai[c§], Yuheng Luo[a], Zesen Wang[a,b], Jinghui Lu[d], Ashanie Herath[a,b], Chaojiang Zhang[a,b], Jia Wang[a,b], Andrew M. Turner[a,b], Baoyu Song[d], Yang Pan[d*], Tao Yang[c,e,f*], Rui Sun[a*], Ryan C. Fortenberry[g*], Ralf I. Kaiser[a,b]*

[a] Department of Chemistry, University of Hawaii at Mānoa, Honolulu, HI 96822, USA

[b] W.M. Keck Laboratory in Astrochemistry, University of Hawaii at Mānoa, Honolulu, HI 96822, USA

[c] State Key Laboratory of Precision Spectroscopy, East China Normal University, Shanghai 200062, P. R. China

[d] National Synchrotron Radiation Laboratory, University of Science and Technology of China, Hefei, Anhui 230029, P. R. China

[e] Xinjiang Key Laboratory of Radio Astrophysics, 150 Science 1-Street, Urumqi, Xinjiang 830011, P. R. China

[f] Collaborative Innovation Center of Extreme Optics, Shanxi University, Taiyuan, Shanxi 030006, P. R. China

[g] Department of Chemistry & Biochemistry, University of Mississippi, University, Oxford, MS 38677, USA.

[§]M.M. and X.B. contributed equally to this work.

*Corresponding authors:

Yang Pan — panyang@ustc.edu.cn

Tao Yang — tyang@lps.ecnu.edu.cn

Rui Sun — ruisun@hawaii.edu

Ryan C. Fortenberry — r410@olemiss.edu

Ralf I. Kaiser — ralfk@hawaii.edu

Downloaded from pubs.acs.org/jpcicd/article-supplement/5463676/pdf/jz6c03291_si_001/ by Ralf Kaiser on 23 November 2026

Material and Methods

Synchrotron

High ionization energy experiments exploiting the vacuum ultraviolet light were conducted at the Shanghai-Hawaii-Hefei Advanced Research Center for Astrochemistry utilizing the Combustion and Flame Beamline (BL03U) of the National Synchrotron Radiation Laboratory (NSRL). The stainless steel ultrahigh vacuum chamber is pumped to 8×10^{-11} Torr by a magnetically levitated turbomolecular pump (Osaka, TG1300M), backed by a second turbomolecular pump (Osaka, TG420M) and further backed by a multistage roots pump (Leybold, Ecodry 40 Plus). A polished silver substrate was affixed to an ultra-high purity copper cold finger interfaced to a two-stage closed-cycle helium refrigerator (Sumitomo Heavy Industries, RDK-415E) capable of reaching temperatures of 5 K. Temperature of the substrate is measured by a cryogenic temperature sensor (Lakeshore, DT-470) and regulated by a programmable temperature controller (Lakeshore, Model 336) with a precision of ± 0.1 K. Once cooled to 5 K, sulfur dioxide (SO_2; Air Liquide; 99.999%) was introduced into the chamber via a glass capillary array aimed at the silver target at a pressure of (2×10^{-8} Torr) for 25 minutes and monitored by laser interferometry with a He–Ne laser (CVI Melles Griot; 25-LHP-230, 632.8 nm) at an incidence angle of 2° and a photodiode (Thorlabs, SM1PD1A) connected to a picoammeter (Keithley 6485).

After deposition, irradiation was conducted isothermally at 5 K at currents of 100 nA for 1 hr using 5 keV electrons produced by an electron gun (SPECS GmbH, EQ 22/35) at an angle of incidence of 0°. After irradiation, temperature-programmed desorption (TPD) was initiated by heating the silver substrate from 5 K to 330 K at a rate of 1.0 K min^{-1}. Subliming material is ionized by synchrotron vacuum ultraviolet light produced by an undulator at the BL03U beamline and the ions are subsequently accelerated and collected by a pulsed reflectron time-of-flight-mass spectrometer (Jordan TOF Products, Inc.) operating with a 2.5 μs pulse width generated by a pulse delay generator (Quantum Composers, 9528) operating at 10 kHz repetition rate. Signal was processed by an amplifier-discriminator (Advanced Research Instruments Corporation) and collected by a multichannel scaler (FAST ComTec, MCS8). Each spectrum contains 0.6 million sweeps in a 3.2 ns bin width, which corresponds to a data collection time of 60 s.

Downloaded from pubs.acs.org/jpcl/article-supplement/5463676/pdf/jz6c03291_si_001/ by Ralf Kaiser on 23 November 2026

W. M. Keck Laboratory

Additional experiments on lower photon energies (11.10 eV, 10.82 eV, 10.49 eV, and 10.20 eV) were performed at the W.M. Keck Laboratory at the University of Hawai'i at Manoa. Here, an ultra-high vacuum stainless steel chamber is pumped down to 10^{-11} Torr by magnetically levitated turbo molecular pumps (Osaka, TG1300MUCWB, TG420MCAB) with rough vacuum backing by an oil-free dry scroll pump (XDS35i, Edwards). Centered inside the stainless-steel chamber is a high purity copper cold finger connected to a closed-cycle helium refrigerator (Sumitomo Heavy Industries, RDK-415E) capable of reaching temperatures as low as 5 K. Sulfur dioxide (SO_2) is introduced into the chamber via a glass capillary array and deposited onto a polished silver wafer affixed to the copper cold head. The gas deposition is monitored by a He-Ne laser (Melles Griot, 25-LHP-230, 632.8 nm) which allows the ice thickness to be calculated by exploiting the refractive index of SO_2 (n = 1.33)[1]. The average ice thickness can be found in Table S2.

After deposition, the infrared spectrum of the pure ice was measured using a Fourier transform infrared (FTIR) spectrometer (Thermo, Nicolet 6700) was used with a range of 6000–500 cm^{-1} and a resolution of 4 cm^{-1}. Subsequently, the ice was irradiated using 5 keV electrons produced from an electron gun (SPECS, EQ PU-22) rasterized over an area of 1.6 cm^2 at 100 nA of current for 60 minutes. During irradiation FTIR spectra were collected and averaged over two-minute intervals to monitor changes in the ice due to the irradiation.

After irradiation, the ices were heated from 5 to 330 K at 1 K min^{-1} in a temperature-programmed desorption (TPD) process. Subliming material entering the gas-phase are then photoionized by pulsed vacuum ultraviolet (VUV) light (30 Hz), generated through resonant four-wave mixing inside a noble gas jet (Krypton or Xenon) pumped by two tunable dye lasers (Sirah, Cobra-Stretch) each pumped by an Nd:YAG laser (Spectra Physics, Quanta Ray Pro 250-30 and 270-30).[2-3] The dyes and wavelengths used to produce VUV light can be found in Table S3. Separation of coincident VUV light was facilitated by a lithium fluoride lens in an off-axis geometry. After production of gas-phase ions, the molecules are detected by a dual microchannel plate (MCP) using a reflectron time-of-flight mass spectrometer (ReToF-MS, Jordan TOF Products). Signals generated by the ions were amplified with a preamplifier (Ortec 9305) and

Downloaded from pubs.acs.org/jpcicd/article-supplement/5463676/pdf/jz6c03291_si_001/ by Ralf Kaiser on 23 November 2026

recorded with a multichannel scaler (FAST ComTec, MCS6A). Each mass spectrum was collected over 2 minutes (3600 sweeps) with an approximate ion arrival time accuracy of 3.2 ns.

FTIR

Experiments were performed in a stainless steel ultrahigh-vacuum chamber held at 8×10^{-11} Torr by a magnetically levitated turbomolecular pump (Osaka, TG420MCAC) backed by an oil-free dry scroll pump (Edwards, GVSP30).[4-5] A two-stage closed-cycle helium compressor (Helix, 9600 Compressor) interfaced to a cold head maintained a temperature of 10.0 ± 0.3 K. Sulfur dioxide (SO_2, Matheson, 99.98%) was deposited at a pressure of 2.7×10^{-7} Torr for 12.7 ± 1.2 minutes via a 2.5 cm diameter glass capillary array onto a cooled reflective silver substrate attached to the cold head. Thickness of the ice was monitored by a He–Ne laser (632.8 nm, Melles Griot, 25-LHP-213) utilizing interferometry, each experimental ice thickness was calculated to be 1250 ± 50 nm. For more information regarding interferometry calculations see Supporting Information.

A Fourier Transform infrared (FTIR) spectrometer (Thermo, Nicolet 6700) covering a range of 6000 to 500 cm^{-1} range at a spectral resolution of 4 cm^{-1} was used with a liquid nitrogen cooled HgCdTe (Thermo, MCT-B) detector. Each sample was irradiated isothermally for 1 hour by 5 keV electrons utilizing an electron gun (SPECS EQ 22-35) at three different beam currents: 100 nA, 1000 nA, and 5000 nA at an angle of incidence of 15°. These currents correspond to a flux of 9.46×10^{12}, 1.89×10^{12}, and 1.89×10^{11} electrons s^{-1} cm^{-2} over an area of 3.7 cm^2 for the 5000, 1000, and 100 nA experiments, respectively. The energetic electrons simulate secondary electrons produced by galactic cosmic rays as they penetrate through interstellar dust grains. According to CASINO simulations[6], the 5000 nA experiment corresponds to a dose of 90 ± 14 eV $molecule^{-1}$ which scales linearly for the 1000 nA and 100 nA doses. By incorporating the density of amorphous SO_2 ice (1.395 g cm^{-3})[1] into CASINO simulations, the maximum penetration depth was found to be 570 ± 50 nm, thus the electrons only interact with the ice and not the silver substrate. FTIR spectra were averaged in two-minute intervals over the course of the irradiation to monitor chemical changes in the ice.

After the irradiation, the ices were heated using temperature-programmed desorption (TPD) from 10 K to 320 K at a rate of 1 K min^{-1} by programmable temperature controller (Lakeshore 336). During TPD, FTIR spectra were once again averaged over two-minute intervals to monitor thermal and chemical changes, while molecules subliming from the surface were analyzed by an

Downloaded from pubs.acs.org/jpcicd/article-supplement/5463676/pdf/jz6c03291_si_001/ by Ralf Kaiser on 23 November 2026

electron-impact ionization quadrupole mass spectrometer (QMS, Balzer, QMG 420) with an electron energy of 100 eV and emission current of 1 mA.

Computations

Calculated adiabatic ionization energies were conducted by optimizing all molecules and harmonic frequencies using CCSD(T)-F12b/cc-pVTZ-F12 (F12-TZ)[7-9] with the MOLPRO 2025.1 quantum chemistry program.[10-11] The adiabatic relative energies are the differences between the F12-TZ energy as well as the harmonic zero-point vibrational energy (ZPE) for a given molecule and the lowest energy isomer of that family. Ionization energies (IEs) are computed in much the same way but with the difference taken between the neutral and the radical cation of the same isomer and corrected for calculation error and the Stark effect (Table S1). Previous IEs have been shown to predict experiment to within −0.05/+0.05 eV and often within 0.01 eV.[12-13] Calculated Cartesian coordinates and frequencies are available in Table S9.

In order to aid in the analysis of the bonding present in the molecules, natural bond orbital (NBO) and molecular orbital analysis were carried out at the B3LYP/aug-cc-pVTZ level of theory[14-18] within Gaussian16[19-21] at the F12-TZ optimized geometries for selected molecules.

Potential Energy Surface Calculations

All equilibrium geometries of reactants, intermediates, products, and transition states were optimized using density functional theory (DFT) in ORCA (version 6.1.0)[22-23], employing the ωB97X-D4[24-25] functional with the def2-TZVPPD[26] basis set. Harmonic vibrational frequency calculations were performed at the same level of theory to obtain zero-point energies (ZPEs) and to confirm the stationary point: local minima were verified by the absence of imaginary frequencies, while transition states were confirmed by the presence of a single imaginary frequency. For all transition states, intrinsic reaction coordinate (IRC)[27-29] calculations were further carried out to ensure correct connectivity between the minima.

An intersystem crossing point (ISC1) between singlet and triplet potential energy surfaces was located using state-averaged complete active space self-consistent field (SA-CASSCF)[30] calculations in Molpro (version 2025.3)[11, 31], with an active space of eight electrons and eight orbitals. The state averaging included the two lowest singlet states and the two lowest triplet states, and state-averaged analytical gradients[32-33] were employed to locate **ISC1**. Since an intersystem

Downloaded from pubs.acs.org/jpcicd/article-supplement/5463676/pdf/jz6c03291_si_001/ by Ralf Kaiser on 23 November 2026

crossing point is not a conventional stationary point on the potential energy surface, standard normal-mode vibrational analysis is not applicable.[34] Instead, following established methodology,[32, 35] an effective Hessian was constructed by projecting out the non-vibrational degrees of freedom, including overall translations, rotations, and the seam-defining direction, yielding the 3N−7 vibrational frequencies associated with **ISC1**. These effective vibrational frequencies were then used to compute the ZPE of **ISC1**.

Single-point electronic energies for all optimized structures were refined using extended multi-state complete active-space second-order perturbation theory (XMS-CASPT2)[36-38] with the same active space and the def2-TZVPPD basis set. The two lowest singlet and triplet states were included in the multi-state treatment to maintain a balanced description of near-degenerate electronic states and to avoid root-flipping problems. A level shift of 0.3 was applied during the CASPT2 calculations to mitigate intruder-state issues, following the recommendations of Roos and Andersson.[39] For a full list of energies and vibrations of the potential energy surface see Table S10.

To further confirm the connectivity between both singlet and triplet reactants, as well as between ISC1 and both singlet and triplet products, a set of 19 smoothly interpolated structures along the full reaction pathway was generated and evaluated at the XMS-CASPT2(8,8)/def2-TZVPPD level (Figure S6). In addition, to assess whether a barrier exists along the reaction path from $S(^1D)$ + SO_2 to the addition intermediate **i1**, a separate scan consisting of 46 smoothly transitioning structures from the separated reactants to **i1** was performed using XMS-CASPT2(8,8). In this case, five singlet states were included in the state-averaged treatment to account for the degeneracy of the $S(^1D)$ atomic state (Figure S7).

Downloaded from pubs.acs.org/jpcld/article-supplement/5463676/pdf/jz6c03291_si_001/ by Ralf Kaiser on 23 November 2026

RESULTS

FTIR

Before irradiation, the infrared spectra recorded over a two-minute interval reveal only vibrational modes of sulfur dioxide: ν_1 (1148 cm^{-1}), ν_2 (530 cm^{-1}), and ν_3 (1325 cm^{-1}) (Figure S4, Table S4). After processing by 5 keV electrons for 1 hour, identification of sulfur trioxide (SO_3) in the 100 nA, 1000 nA, and 5000 nA experiments was provided by the S=O asymmetric stretch (ν_3, 1402 and 1388 cm^{-1}) and the S=O symmetric stretch (ν_1, 1074 cm^{-1}). The 5000 nA experiment reveals the highest concentration of SO_3 at 8.8×10^{16} molecules cm^{-2}—over four times the amount observed in the 100 nA experiment. While the formation of SO_3 occurs in all doses, the 100 nA experiment contains additional vibrational modes associated with the γ-phase of SO_3. This polymeric phase of SO_3, which contains the unit cell of $(SO_3)_3$, has previously been detected in irradiation experiments of pure SO_2 ices.[40] Here, several characteristic vibrations identify the trimer, including ν_6 (603 cm^{-1}), ν_3 (724 cm^{-1}), ν_{15} (850 cm^{-1}), ν_1 (1312 cm^{-1}), among others.

During temperature-programmed desorption, the substrate warms by 1 K min^{-1} to 320 K. The residue remaining at 320 K shows absorptions associated with $(SO_3)_3$ in the 100 nA experiment, with an S=O stretching mode associated with sulfates at 1112 cm^{-1}.[41] The 1000 and 5000 nA experiments can produce additional products that inhibit the polymerization of SO_3. Therefore, this material is only detectable in the 100 nA experiment.

Time-resolved FTIR

Having identified products such as SO_3 (**3a**) and $(SO_3)_3$ in the irradiated ices, integrating the corresponding absorptions during the irradiation allows derivation of a kinetic scheme and the corresponding rate constants (*k*) for their formation (Figure S5, Table S5). Column densities of SO_2, SO_3, and γ-phase SO_3 were calculated utilizing band strengths (A) for ν_2 (1149 cm^{-1}, $A = 2.2 \times 10^{18}$)[42], ν_3 (1380 cm^{-1}, $A = 2.2 \times 10^{17}$)[43], and an estimated band strength of ν_{15} (842 cm^{-1}, $A = 2.2 \times 10^{16}$), respectively.

The kinetic scheme allowed the fitting of the time-resolved column densities during irradiation. These data suggest the destruction of SO_2 occurs in three different pathways: first-order decomposition into sulfur monoxide (SO, **1**) and atomic oxygen [Reaction 1], radical-neutral addition of atomic oxygen to SO_2, and a bimolecular reaction of two SO_2 molecules forming SO_3 and SO [Reaction 3].

Downloaded from pubs.acs.org/jpcicd/article-supplement/5463676/pdf/jz6c03291_si_001/ by Ralf Kaiser on 23 November 2026

$$SO_2 \rightarrow SO + O \quad \text{[Reaction 1]}$$

$$SO_2 + O \rightarrow SO_3 \quad \text{[Reaction 2]}$$

$$SO_2 + SO_2 \rightarrow SO_3 + SO \quad \text{[Reaction 3]}$$

These reactions amount to a total of 3.9×10^{17} sulfur dioxide molecules destroyed. The dominant destruction of SO_2 is through Reaction 3, which contributes 71% of the total processed sulfur dioxide in the 5000 nA experiment. Consequently, this reaction is the primary formation mechanism to produce SO_3 in the ice. The generation of SO_3 was dose dependent with the 5000 nA experiment containing the maximum column density of 8.8×10^{16} molecules cm^{-2}. Interestingly, the SO_2 ice approaches a steady state in the 1000 and 5000 nA experiments where SO_2 reforms by radical-radical recombination of SO and O [Reaction 4] and destruction of SO_3, producing SO_2 and atomic oxygen [Reaction 5].

$$SO + O \rightarrow SO_2 \quad \text{[Reaction 4]}$$

$$SO_3 \rightarrow SO_2 + O \quad \text{[Reaction 5]}$$

This process is most apparent in the 5000 nA experiment where the SO_2 and SO_3 fit no longer change appreciably after 1000 seconds. The equilibria between the sulfur oxides could be reached in molecular clouds of approximately 1×10^7 years. Increases in dose indicate the destruction of SO_3 to form other products [Reaction 6] occurs; however, these species are not directly observable in the infrared spectra. The formation of γ-phase SO_3 is well fit by consecutive addition of SO_3 to form the dimer [Reaction 7] and the trimer unit cell [Reaction 8].

$$SO_3 \rightarrow \text{Products} \quad \text{[Reaction 6]}$$

$$SO_3 + SO_3 \rightarrow (SO_3)_2 \quad \text{[Reaction 7]}$$

$$(SO_3)_2 + SO_3 \rightarrow (SO_3)_3 \quad \text{[Reaction 8]}$$

The latent onset of γ-phase SO_3 in the 100 nA indicates a critical concentration of SO_3 necessary to facilitate the formation of the polymeric phase. The lack of this material in the 1000 nA and 5000 nA experiments could arise from the rapid destruction of the polymer or from additional species produced in the ice inhibiting the polymerization from occurring.

Downloaded from pubs.acs.org/jpcicd/article-supplement/5463676/pdf/jz6c03291_si_001/ by Ralf Kaiser on 23 November 2026

PI-ReToF-MS: Additional Detections

***m/z* = 32**

Beginning with *m/z* = 32, no signal is observed during TPD with a photon energy of 13.00 eV, suggesting molecular oxygen (O_2, *m/z* = 32, IE = 12.0697 ± 0.0002)[44] is not detected under these experimental conditions (Figure S8), indicating SO_2 is not a significant source of molecular oxygen in interstellar grains.

***m/z* = 48**

Similarly, at *m/z* = 48, no signal is observed (Figure S9) suggesting SO (**4**) and ozone (O_3; IE = 12.70 ± 0.03)[45] do not persist during temperature-programmed desorption.[45] This lack of detection is corollary to the lack of evidence for SO and O_3 in the FTIR. The lack of SO **4** could be due to its diradical character ($X\ ^3\Sigma^-$), thus during desorption, SO undergoes many collisions before being released and could undergo additional reactions effectively locking this material within the ice matrix.

***m/z* = 64**

Three isomers are calculated for sulfur dioxide (SO_2, **5a-5c**) including peroxysulfide (SOO, **5b**) and cyclic sulfur dioxide (cyc-SO_2, **5c**). At 13.00 eV all isomers can be ionized and at 12.00 eV only **5b** and **5c** can be ionized. TPD profiles (Figure S10) show signal at 13.00 eV and no signal at 12.00 eV; thus, the only SO_2 material observed in these experiments derives from the reagent material (**5a**) and isomerization of SO_2 to peroxysulfide **5b** or the cyc-SO_2 **5c** is not detected under these conditions.

***m/z* = 80**

Two chemical formulae are associated with *m/z* = 80, SO_3 (**3a-3e**) and S_2O (**6a-6c**). At 13.00 eV four sublimation events occur (Figure S11A). All isomers of SO_3 (**3**) and S_2O (**6**) can be ionized. Tuning the photon energy to 12.00 eV, all species of SO_3 and S_2O can be ionized except the most symmetric isomer of SO_3 (**3a**) (Figure S11A). At this photon energy, **peak 1** is no longer observed and thus can only be attributed to SO_3 (**3a**). Next the photon energy is tuned to 11.16 eV (Figure S11B) which is below the ionization energy of sulfur oxide peroxide (OSOO, **3b**). The disappearance of **peak 4** confirms the presence of OSOO **3b**. Next, the experiment at 10.82 eV

Downloaded from pubs.acs.org/jpcicd/article-supplement/5463676/pdf/jz6c03291_si_001/ by Ralf Kaiser on 23 November 2026

(Figure S11C) can ionize S_2O **6a**-**6c** and SO_3 **3d**-**3e** but not SO_3 **3c**. Since **peak 3** is no longer detected, this peak can only be attributed to 1,2,3-dioxathiirane 3-oxide (cyc-S(O)OO, **3c**). Lastly, tuning the photon energy from 10.82 eV to 10.49 eV, only disulfur monoxide (OSS, **6a**) can no longer be ionized. At this energy, no sublimation event is recorded, thus the final **peak 2** is attributed to disulfur oxide (S_2O **6a**).

***m/z* = 96**

Since the signal at 12.00 eV could contain SSO_2 **1a** and SO_4 **2b**, the fragmentation channels of SO_4^+ were theoretically investigated (Figure S12), which reveal SO_2^+ plus O_2 and SO_2 plus O_2^+. On this potential energy surface, SO_4^+ is noted to have a nearly energetically degenerate saddle point for ionization before fragmentation. Both pathways are highly exoergic, where forming SO_2^+ results in an exoergicity of −257 kJ mol^{-1} and the more favored loss is the formation of O_2^+ that is exoergic −287 kJ mol^{-1}. Since no O_2^+ is detected via *m/z* = 32 nor SO_2^+ at *m/z* = 64 at 225 K, the signal at 11.43 eV and 12.00 eV can only be attributed to SSO_2 **1a** (Figure S8 and S10).

Downloaded from pubs.acs.org/jpcld/article-supplement/5463676/pdf/jz6c03291_si_001/ by Ralf Kaiser on 23 November 2026

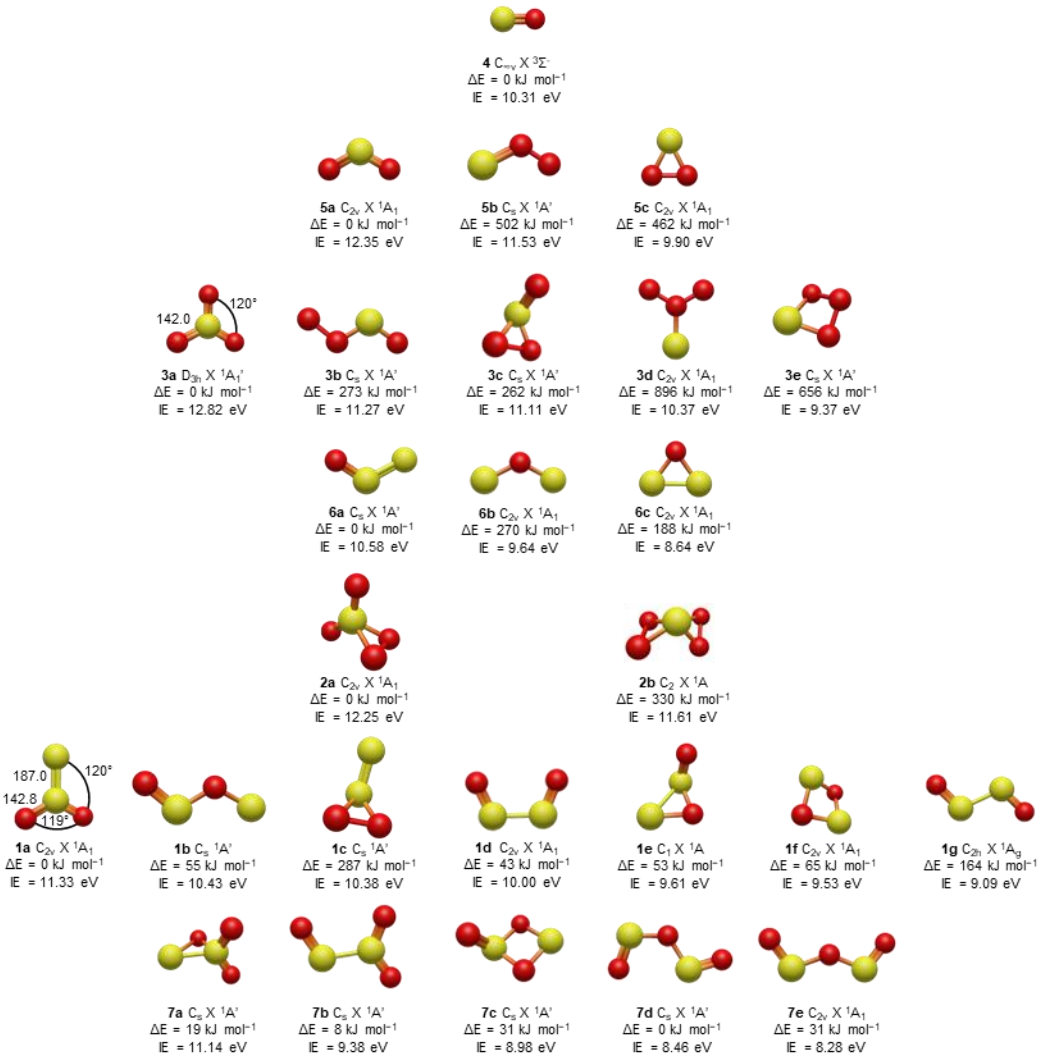

Figure S1. Sulfoxides (S_xO_y, where x = 1-2 and y = 1-4) isomers with calculated adiabatic ionization energies (IE) and relative energy (ΔE) calculated at the CCSD(T)-F12/cc-pVTZ-F12 level of theory.

Downloaded from pubs.acs.org/jpcicd/article-supplement/5463676/pdf/jz6c03291_si_001/ by Ralf Kaiser on 23 November 2026

Table S1. List of relative energies, adiabatic ionization energies (IEs) and comparison with experimental energies using the CCSD(T)-F12/cc-pVTZ-F12 (F12-TZ) level of theory.

Chemical Formulae	Molecule	Relative Energy (kJ mol^{-1})	Calculated IE (eV)	Experimental IE (eV)[a]
SO	**4**	--	10.31	10.294
SO_2	**5a**	0	12.35	12.349
	5b	502	11.53	
	5c	462	9.90	
SO_3	**3a**	0	12.82	12.8
	3b	273	11.27	
	3c	262	11.11	
	3d	896	10.37	
	3e	656	9.37	
S_2O	**6a**	0	10.58	10.584
	6b	270	9.64	
	6c	188	8.64[b]	
SO_4	**2a**	0	12.25	
	2b	330	11.61	
S_2O_2	**1a**	0	11.33	
	1b	55	10.43	
	1c	287	10.38	
	1d	43	10.00	
	1e	53	9.61	
	1f	65	9.53	
	1g	164	9.09	
S_2O_3	**7a**	19	11.14	
	7b	8	9.38	
	7c	31	8.98	
	7d	0	8.46	
	7e	31	8.28	

[a] Referenced IEs are from compiled data from *NIST Chemistry WebBook*[46]

[b]The cation reverts back to SSO^+.

Downloaded from pubs.acs.org/jpcicd/article-supplement/5463676/pdf/jz6c03291_si_001/ by Ralf Kaiser on 23 November 2026

Table S2. Experimental parameters for the sulfur-bearing ices.

Experiment	Ice Composition	Irradiation Current (nA)	Irradiation Time (min)	Energy (eV)	Average Ice Thickness (nm)
FTIR Simulation Experiments					
1	SO_2	100	60	-	1250 ± 50
2	SO_2	1000	60	-	
3	SO_2	5000	60	-	
W.M. Keck Experiments					
4	SO_2	100	60	11.10	1140 ± 60
5	SO_2	100	60	10.82	
6	SO_2	100	60	10.49	
7	SO_2	100	60	10.20	
Hefei Synchrotron					
8	SO_2	100	60	13.00	930 ± 30
9	SO_2	100	60	12.00	
10	SO_2	100	60	11.16	

Downloaded from pubs.acs.org/jpcicd/article-supplement/5463676/pdf/jz6c03291_si_001/ by Ralf Kaiser on 23 November 2026

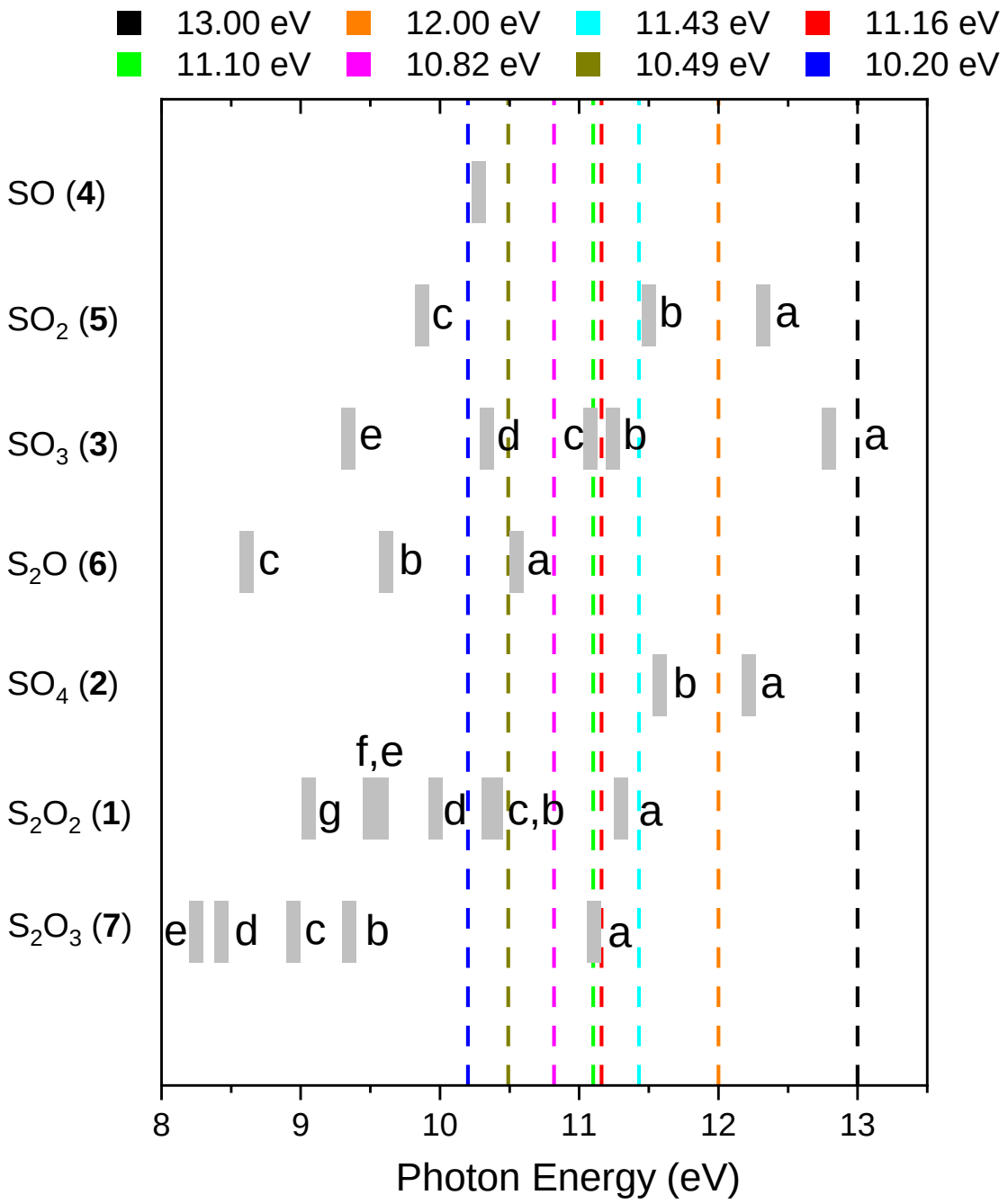

Figure S2. Compilation of ionization energies of each molecule corrected for computational error and the Stark effect (gray bars) and photon energies (dashed colored line) used to selectively ionize each species. See Table S1 for a list of calculated ionization energy ranges.

Downloaded from pubs.acs.org/jpcicd/article-supplement/5463676/pdf/jz6c03291_si_001/ by Ralf Kaiser on 23 November 2026

Table S3. Parameters for the generation of VUV light utilizing difference four-wave mixing. The resulting photon energy has an uncertainty of less than 0.001 eV.

Experiment	Medium	ω_{VUV}	ω_1 (nm)	YAG 1 Wavelength (nm)	ω_1 Dye	YAG 2 Wavelength (nm)	ω_2 (nm)	ω_2 Dye	Energy (eV)
4	Xenon	$2\omega_1 + \omega_2$	249.628	355	Coumarin 503	1064	1064[a]	-	11.10
5	Krypton	$2\omega_1 - \omega_2$	202.316	532	Rhodamine 610/640	532	739.55	LDS 751	10.82
6	Xenon	$3\omega_1$	355	355	-	-	-	-	10.49
7	Krypton	$2\omega_1 - \omega_2$	202.316	532	Rhodamine 610/640	532	845.71	LDS 863	10.20

[a]Nd:YAG harmonic/fundamental

Downloaded from pubs.acs.org/jpclcd/article-supplement/5463676/pdf/jz6c03291_si_001/ by Ralf Kaiser on 23 November 2026

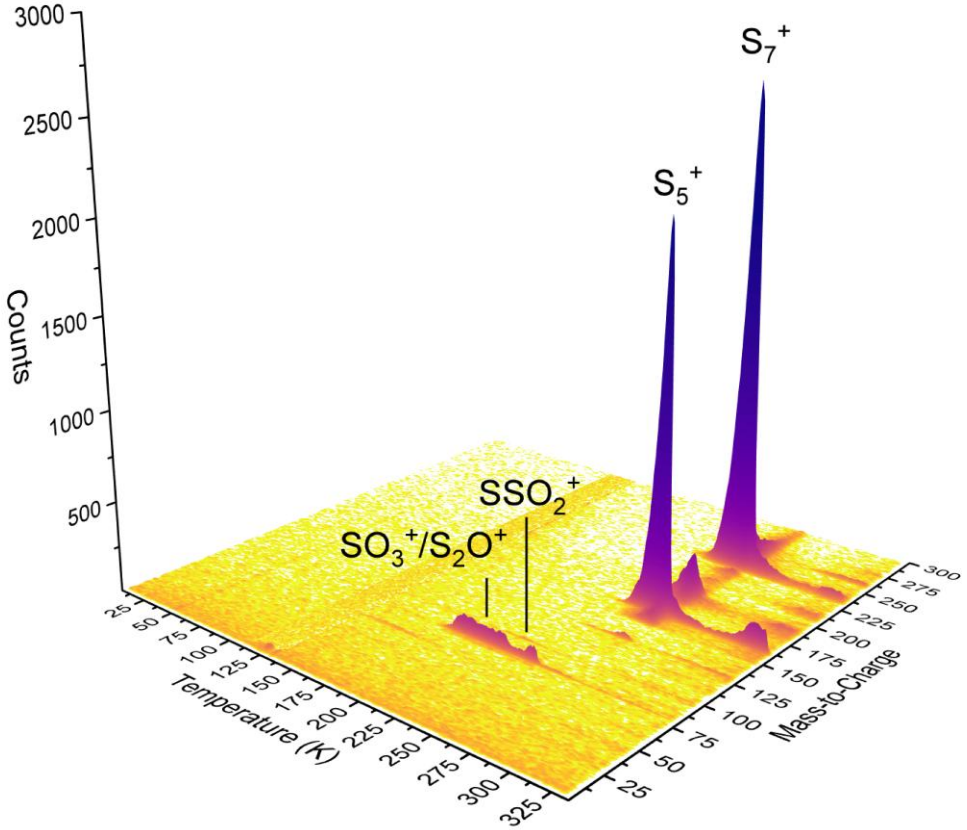

Figure S3. All recorded masses during TPD (5-330 K) of the 12.00 eV irradiated SO_2 ices. Major peaks are labeled along with peaks of interest.

Downloaded from pubs.acs.org/jpcicd/article-supplement/5463676/pdf/jz6c03291_si_001/ by Ralf Kaiser on 23 November 2026

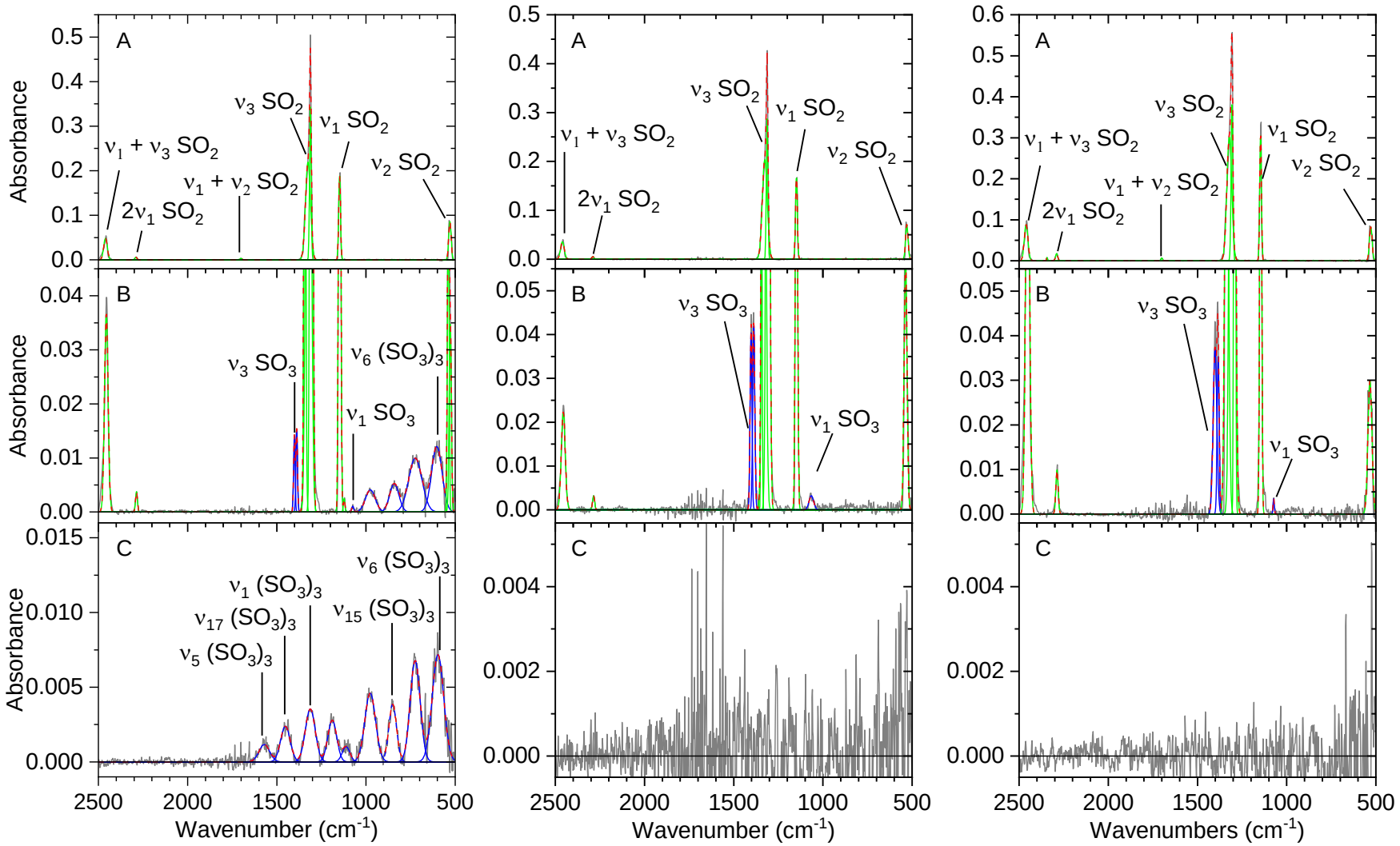

Figure S4. Infrared spectra of SO_2 pure ices in the 100 (left), 1000 (center), 5000 (right) nA experiments. The top row indicates (A) before irradiation, (B) the middle row after irradiation and (C) the bottom row the resulting residue at 320 K.

Downloaded from pubs.acs.org/jpclcd/article-supplement/5463676/pdf/jz6c03291_si_001/ by Ralf Kaiser on 23 November 2026

Table S4. Infrared Absorption Features Before and After Irradiation of 100, 1000, and 5000 nA for 1 hr (10 K) and in the Residue at 320 K of the Sulfur Dioxide (SO_2) Ices

Before (cm^{-1})	After (cm^{-1})	Residue (cm^{-1})	Assignment	Carrier	Dose (nA)	References
2460	2456		$\nu_1 + \nu_3$	SO_2	100, 1000, 5000	[40]
2289	2287		$2\nu_1$	SO_2	100, 1000, 5000	[40]
1697			$\nu_1 + \nu_2$	SO_2	100, 5000	[40]
		1574	ν_5	$(SO_3)_3$	100	[40]
		1452	ν_{17}	$(SO_3)_3$	100	[40]
	1402, 1388		ν_3	SO_3	100, 1000, 5000	[40]
1325, 1312	1343, 1322, 1306		ν_3	SO_2	100, 1000, 5000	[40]
		1312	ν_1	$(SO_3)_3$	100	[40]
		1189	ν_{11}	$(SO_3)_3$	100	[40]
1148	1148		ν_1	SO_2	100, 1000, 5000	[40]
1122	1122		ν_1	$S^{16}O^{18}O$	100, 1000, 5000	[40]
		1112	ν(S=O)	Ag_2SO_4	100	[47]
	1074		ν_1	SO_3	100, 1000, 5000	[40]
	976	977	ν_{16}	$(SO_3)_3$	100	[40]
	842	850	ν_{15}	$(SO_3)_3$	100	[40]
	724	724	ν_3	$(SO_3)_3$	100	[40]
	603	597	ν_6	$(SO_3)_3$	100	[40]
530	539, 528		ν_2	SO_2	100, 1000, 5000	[40]

Downloaded from pubs.acs.org/jpcld/article-supplement/5463676/pdf/jz6c03291_si_001/ by Ralf Kaiser on 23 November 2026

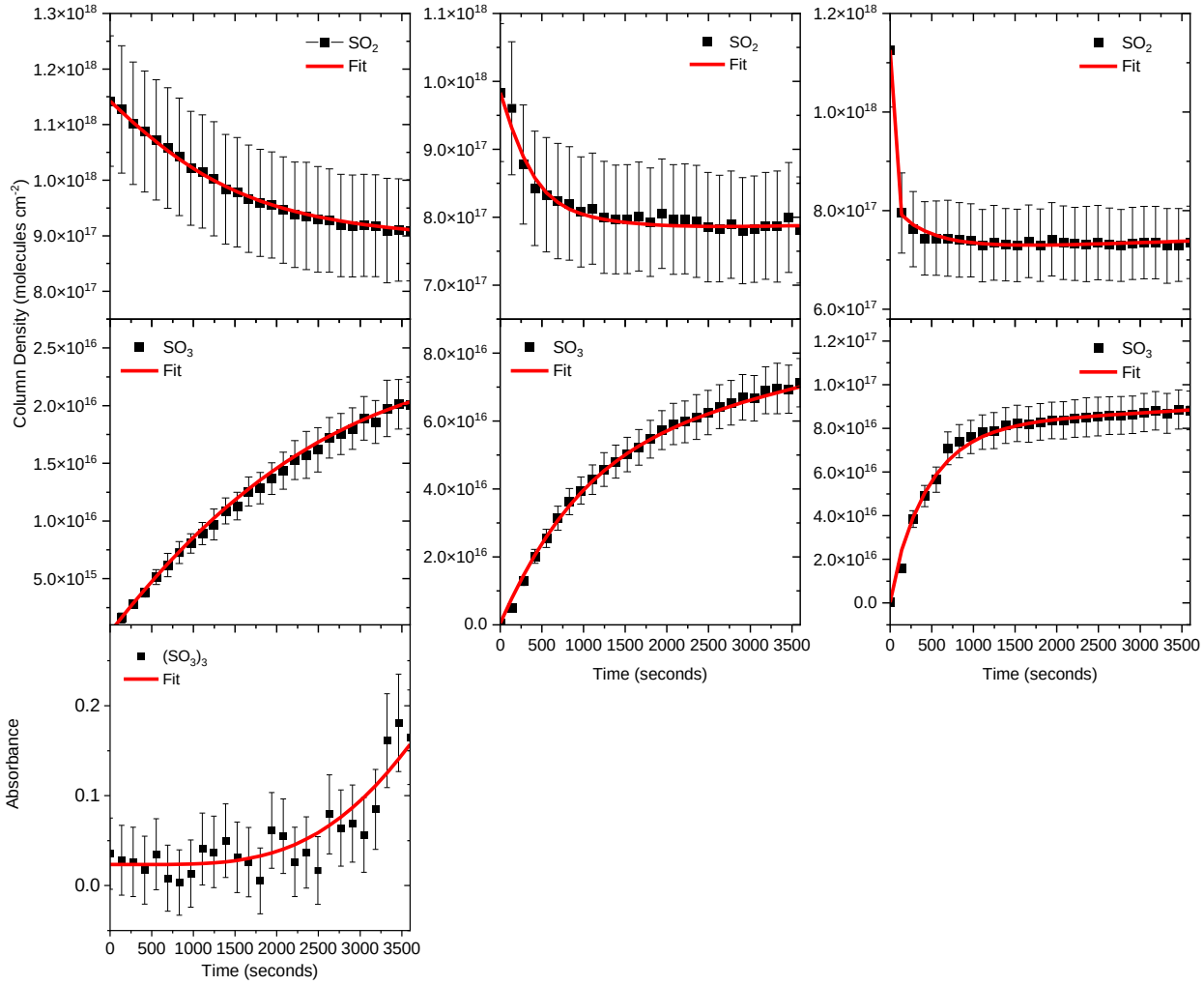

Figure S5. Changes in the FTIR spectra during irradiation of SO_2, SO_3, and $(SO_3)_3$. The column density (molecules cm^{-2}) and absorbance (black) are plotted against kinetic fits (red) in the 100 nA (left), 1000 nA (middle), and 5000 nA (right) SO_2 ices.

Downloaded from pubs.acs.org/jpcicd/article-supplement/5463676/pdf/jz6c03291_si_001/ by Ralf Kaiser on 23 November 2026

Table S5. Rate Constants Derived from Iterative Fitting of Reaction Scheme

Rate Constant	Reaction		Dose			Units
			100 nA	1000 nA	5000 nA	
k_1	SO_2	$\rightarrow SO + O(^3P/^1D)$	$1.07 \pm 0.03 \times 10^{-4}$	$2.8 \pm 0.3 \times 10^{-4}$	$5.7 \pm 0.2 \times 10^{-3}$	s^{-1}
k_2	$SO_2 + O(^3P/^1D)$	$\rightarrow SO_3$	$3.8 \pm 0.5 \times 10^{-24}$	$2.0 \pm 0.1 \times 10^{-22}$	$1.0 \pm 0.5 \times 10^{-22}$	cm^2 $molecule^{-1}$ s^{-1}
k_3	$(SO_2)_2$	$\rightarrow SO + SO_3$	$7.16 \pm 0.05 \times 10^{-24}$	$5.7 \pm 0.3 \times 10^{-23}$	$2.27 \pm 0.03 \times 10^{-22}$	cm^2 $molecule^{-1}$ s^{-1}
k_4	$SO + O(^3P/^1D)$	$\rightarrow SO_2$	$2.5 \pm 0.7 \times 10^{-21}$	$2.5 \pm 0.2 \times 10^{-20}$	$5.1 \pm 0.1 \times 10^{-20}$	cm^2 $molecule^{-1}$ s^{-1}
k_5	SO_3	$\rightarrow SO_2 + O$	$3.3 \pm 0.1 \times 10^{-5}$	$7.0 \pm 0.3 \times 10^{-4}$	$1.55 \pm 0.05 \times 10^{-4}$	s^{-1}
k_6	SO_3	$\rightarrow$ Products	-	$1.1 \pm 0.2 \times 10^{-4}$	$9 \pm 1 \times 10^{-3}$	s^{-1}
k_7	$SO_3 + SO_3$	$\rightarrow (SO_3)_2$	$3.3 \pm 0.2 \times 10^{-21}$	-	-	cm^2 $molecule^{-1}$ s^{-1}
k_8	$SO_3 + (SO_3)_2$	$\rightarrow (SO_3)_3$	$3.0 \pm 0.4 \times 10^{-20}$	-	-	cm^2 $molecule^{-1}$ s^{-1}

Downloaded from pubs.acs.org/jpcicd/article-supplement/5463676/pdf/jz6c03291_si_001/ by Ralf Kaiser on 23 November 2026

Table S6. Summary of Natural Bond Order calculations of SO_3 (**3a**) using the geometry computed at the CCSD(T)-F12/cc-pVTZ-F12 (F12-TZ) level of theory.

SO_3 (3a)

Bond Type	**Occupancy**	**Atom contribution**	**Interpretation**
π(S–O)	1.99815	O1 75.43% S_c 24.57%	Localized S–O π bond for specific resonance structure
σ(S–O)	1.98489	O1 64.46% S_c 35.54%	Polarized S–O σ bond
σ(S–O)	1.98489	S_c 35.54% O2 64.46%	Polarized S–O σ bond
σ(S–O)	1.98489	S_c 35.54% O3 64.46%	Polarized S–O σ bond
delocalized O/O*	1.95946	O2 50.00% O3 50.00%	Occupied antibonding-type O/O *p* combination
delocalized O/O	1.33869	O2 50.00% O3 50.00%	Occupied bonding-type O/O *p* combination

Note. S_c defines the central sulfur atom.

Downloaded from pubs.acs.org/jpcicd/article-supplement/5463676/pdf/jz6c03291_si_001/ by Ralf Kaiser on 23 November 2026

Table S7. Summary of Natural Bond Order calculations of SSO_2 (**1a**) using the geometry computed at the CCSD(T)-F12/cc-pVTZ-F12 (F12-TZ) level of theory.

SSO_2 (1a)

Bond Type	**Occupancy**	**Atom contribution**	**Interpretation**
σ(S–S)	1.96739	S_t 40.61%; S_c 59.39%	Polarized S–S σ bond
π(S–S)	1.99567	S_t 66.86%; S_c 33.14%	Localized S–S π bond
σ(S–O)	1.98812	S_c 35.17%; O1 64.83%	Polarized S–O σ bond
σ(S–O)	1.98812	S_c 35.17%; O2 64.83%	Polarized S–O σ bond

Note. S_c and S_t define the central and terminal sulfur atom respectively.

Downloaded from pubs.acs.org/jpcicd/article-supplement/5463676/pdf/jz6c03291_si_001/ by Ralf Kaiser on 23 November 2026

Table S8. Full data calculated for Natural Bond Order calculations of SO_3 (**3a**) and SSO_2 (**1a**) using the geometry computed at the CCSD(T)-F12/cc-pVTZ-F12 (F12-TZ) level of theory.

SO_3 (3a)		
NBO label and occupancy	**Component and hybrid character**	**Coefficients**
BD(1) O1 - S2 Occupancy 1.98489	64.46% 0.8029* O1 s(21.86%) p3.53(77.08%) d0.05(1.03%) f0.00(0.03%)	-0.0000 -0.4675 0.0045 0.0002 -0.0010 0.0000 0.0000 0.0000 0.0000 0.8777 -0.0214 -0.0014 0.0016 0.0000 0.0000 0.0000 0.0000 0.0000 0.0000 0.0000 0.0000 0.0000 0.0000 0.0000 0.0000 0.0000 0.0902 -0.0059 0.0017 0.0455 -0.0074 0.0005 0.0000 0.0000 0.0000 0.0000 -0.0090 -0.0015 0.0000 0.0000 0.0000 0.0000 0.0000 0.0000 -0.0154 0.0003
BD(1) O1 - S2 Occupancy 1.98489	35.54% 0.5961* S2 s(33.26%) p1.97(65.41%) d0.04(1.32%) f0.00(0.01%)	0.0000 0.0001 -0.5767 0.0022 0.0000 -0.0000 -0.0000 0.0000 0.0000 -0.0000 0.0000 -0.0001 -0.8061 -0.0645 0.0076 -0.0002 0.0000 0.0000 0.0000 0.0000 0.0000 0.0000 0.0000 0.0000 0.0000 0.0000 0.0000 0.0000 0.0000 0.0000 -0.1115 -0.0111 -0.0011 -0.0202 -0.0156 0.0032 0.0000 0.0000 -0.0000 -0.0000 0.0057 0.0004 0.0000 0.0000 0.0000 0.0000 0.0000 0.0000 0.0094 0.0012
BD(2) O1 - S2 Occupancy 1.99815	75.43% 0.8685* O1 s(0.00%)p1.00(99.22%)d0.01(0. 75%) f0.00(0.03%)	0.0000 0.0000 0.0000 0.0000 0.0000 0.0000 0.0000 0.0000 0.0000 0.0000 0.0000 0.0000 0.0000 0.9961 0.0067 -0.0004 -0.0003 0.0000 0.0000 0.0000 0.0000 0.0000 0.0000 -0.0867 -0.0047 -0.0011 0.0000 0.0000 0.0000 0.0000 0.0000 0.0000 -0.0078 -0.0012 0.0000 0.0000 0.0000 0.0000 -0.0140 0.0004 0.0000 0.0000 0.0000 0.0000 0.0000 0.0000
BD(2) O1 - S2 Occupancy 1.99815	24.57% 0.4957* S2 s(0.00%)p1.00(95.81%)d0.04(4. 09%) f0.00(0.10%)	0.0000 0.0000 0.0000 0.0000 0.0000 0.0000 0.0000 0.0000 0.0000 0.0000 0.0000 0.0000 0.0000 0.0000 0.0000 0.0000 0.0000 0.9779 -0.0403 0.0116 -0.0034 0.0000 0.0000 0.0000 0.0000 0.0000 0.0000 -0.2019 0.0113 0.0039 0.0000 0.0000 0.0000 0.0000 0.0000 0.0000 -0.0206 0.0092 0.0000 0.0000 0.0000 0.0000 -0.0222 0.0039 0.0000 0.0000 0.0000 0.0000 0.0000 0.0000
BD(1) S2 - O3 Occupancy 1.98489	35.54% 0.5961* S2 s(33.26%)p1.97(65.41%)d0.04(1 .32%) f0.00(0.01%)	-0.0000 -0.0001 0.5767 -0.0022 -0.0000 0.0000 0.0001 0.6981 0.0558 -0.0065 0.0002 -0.0000 -0.4031 -0.0322 0.0038 -0.0001 0.0000 0.0000 0.0000 0.0000 0.0000 0.0966 0.0096 0.0010 0.0000 0.0000 0.0000 0.0000 0.0000 0.0000 -0.0558 -0.0056 -0.0006 0.0202 0.0156 -0.0032 0.0000 0.0000 -0.0050 -0.0003 0.0029 0.0002 0.0000 0.0000 0.0000 0.0000 0.0000 0.0000 -0.0094 -0.0012
BD(1) S2 - O3 Occupancy 1.98489	64.46% 0.8029* O3 s(21.86%)p3.53(77.08%)d0.05(1 .03%) f0.00(0.03%)	0.0000 0.4675 -0.0045 -0.0002 0.0010 -0.7601 0.0185 0.0012 -0.0014 0.4388 -0.0107 -0.0007 0.0008 0.0000 0.0000 0.0000 0.0000 -0.0781 0.0051 -0.0015 0.0000 0.0000 0.0000 0.0000 0.0000 0.0000 0.0451 -0.0029 0.0009 -0.0455 0.0074 -0.0005 0.0000 0.0000 0.0078 0.0013 -0.0045 -0.0007 0.0000 0.0000 0.0000 0.0000 0.0000 0.0000 0.0154 -0.0003
BD(1) S2 - O4 Occupancy 1.98489	35.54% 0.5961* S2 s(33.26%)p1.97(65.41%)d0.04(1 .32%) f0.00(0.01%)	-0.0000 -0.0001 0.5767 -0.0022 -0.0000 0.0000 -0.0001 -0.6981 -0.0558 0.0065 -0.0002 -0.0000 -0.4031 -0.0322 0.0038 -0.0001 0.0000 0.0000 0.0000 0.0000 0.0000 -0.0966 -0.0096 -0.0010 0.0000 0.0000 0.0000 0.0000 0.0000 0.0000 -0.0558 -0.0056 -0.0006 0.0202 0.0156 -0.0032 0.0000 0.0000 0.0050 0.0003

Downloaded from pubs.acs.org/jpcicd/article-supplement/5463676/pdf/jz6c03291_si_001/ by Ralf Kaiser on 23 November 2026

		0.0029 0.0002 0.0000 0.0000 0.0000 0.0000 0.0000 -0.0000 -0.0094 -0.0012
BD(1) S2 - O4 Occupancy 1.98489	64.46% 0.8029* O4 s(21.86%)p3.53(77.08%)d0.05(1 .03%) f0.00(0.03%)	0.0000 0.4675 -0.0045 -0.0002 0.0010 0.7601 -0.0185 -0.0012 0.0014 0.4388 -0.0107 -0.0007 0.0008 0.0000 0.0000 0.0000 0.0000 0.0781 -0.0051 0.0015 0.0000 0.0000 0.0000 0.0000 0.0000 0.0000 0.0451 -0.0029 0.0009 -0.0455 0.0074 -0.0005 0.0000 0.0000 -0.0078 -0.0013 -0.0045 -0.0007 0.0000 0.0000 0.0000 0.0000 -0.0000 0.0000 0.0154 -0.0003
BD*(1) O3 - O4 Occupancy 1.95946	50.00% 0.7071* O3 s(0.00%)p1.00(99.07%)d0.01(0. 90%) f0.00(0.03%)	0.0000 0.0000 0.0000 0.0000 0.0000 0.0000 0.0000 0.0000 0.0000 0.0000 0.0000 0.0000 0.0000 0.9951 0.0242 -0.0040 -0.0017 0.0000 0.0000 0.0000 -0.0740 -0.0021 0.0024 0.0584 0.0085 -0.0007 0.0000 0.0000 0.0000 0.0000 0.0000 0.0000 -0.0078 -0.0001 0.0000 0.0000 0.0000 0.0000 0.0060 -0.0004 -0.0133 0.0024 0.0000 0.0000 0.0000 0.0000
BD*(1) O3 - O4 Occupancy 1.95946	50.00% -0.7071* O4 s(0.00%)p1.00(99.07%)d0.01(0. 90%) f0.00(0.03%)	-0.0000 -0.0000 -0.0000 -0.0000 -0.0000 -0.0000 -0.0000 -0.0000 -0.0000 -0.0000 -0.0000 -0.0000 -0.0000 0.9951 0.0242 -0.0040 -0.0017 -0.0000 -0.0000 -0.0000 0.0740 0.0021 -0.0024 0.0584 0.0085 -0.0007 -0.0000 -0.0000 -0.0000 -0.0000 -0.0000 -0.0000 -0.0078 -0.0001 -0.0000 -0.0000 -0.0000 -0.0000 0.0060 -0.0004 0.0133 -0.0024 -0.0000 -0.0000 -0.0000 -0.0000
BD(1) O3 - O4 Occupancy 1.33869	50.00% 0.7071* O3 s(0.00%)p1.00(99.07%)d0.01(0. 90%) f0.00(0.03%)	0.0000 0.0000 0.0000 0.0000 0.0000 0.0000 0.0000 0.0000 0.0000 0.0000 0.0000 0.0000 0.0000 0.9951 0.0242 -0.0040 -0.0017 0.0000 0.0000 0.0000 -0.0740 -0.0021 0.0024 0.0584 0.0085 -0.0007 0.0000 0.0000 0.0000 0.0000 0.0000 0.0000 -0.0078 -0.0001 0.0000 0.0000 0.0000 0.0000 0.0060 -0.0004 -0.0133 0.0024 0.0000 0.0000 0.0000 0.0000
BD(1) O3 - O4 Occupancy 1.33869	50.00% 0.7071* O4 s(0.00%)p1.00(99.07%)d0.01(0. 90%) f0.00(0.03%)	-0.0000 -0.0000 -0.0000 -0.0000 -0.0000 -0.0000 -0.0000 -0.0000 -0.0000 -0.0000 -0.0000 -0.0000 -0.0000 0.9951 0.0242 -0.0040 -0.0017 -0.0000 -0.0000 -0.0000 0.0740 0.0021 -0.0024 0.0584 0.0085 -0.0007 -0.0000 -0.0000 -0.0000 -0.0000 -0.0000 -0.0000 -0.0078 -0.0001 -0.0000 -0.0000 -0.0000 -0.0000 0.0060 -0.0004 0.0133 -0.0024 -0.0000 -0.0000 -0.0000 -0.0000
SSO_2 (1a)		
BD(1) S1 - S2 Occupancy 1.96739	40.61% 0.6372* S1 s(9.64%)p9.19(88.59%)d0.17(1. 68%) f0.01(0.08%)	0.0000 0.0000 0.3105 0.0034 0.0001 -0.0014 0.0000 0.0000 0.0000 0.0000 0.0000 0.0000 -0.0000 0.0000 0.0000 0.0000 -0.0000 -0.9402 0.0449 -0.0022 -0.0007 0.0000 0.0000 0.0000 0.0000 0.0000 0.0000 -0.0000 -0.0000 0.0000 0.0085 0.0048 -0.0006 0.1283 -0.0092 0.0136 -0.0281 0.0042 0.0000 0.0000 0.0000 0.0000 -0.0041 -0.0038 0.0000 0.0000 0.0000 0.0000 -0.0000 0.0000
BD(1) S1 - S2 Occupancy 1.96739	59.39% 0.7707* S2 s(35.59%)p1.77(62.98%)d0.04(1 .41%) f0.00(0.02%)	0.0000 -0.0000 0.5949 0.0448 0.0005 0.0007 0.0000 0.0000 0.0000 0.0000 0.0000 0.0000 0.0000 -0.0000 -0.0000 0.0000 0.0001 0.7929 -0.0303 0.0114 -0.0120 0.0000 0.0000 0.0000 0.0000 0.0000 0.0000 0.0000 0.0000 -0.0000 -0.0470 0.0055 -0.0025 -0.1083 -0.0061 -0.0098 0.0119 0.0023 0.0000 0.0000 0.0000 0.0000 -0.0031 0.0021 0.0000 0.0000 0.0000 0.0000 0.0000 -0.0000
BD(2) S1 - S2 Occupancy 1.99567	66.86% 0.8177* S1 s(0.00%)p1.00(98.92%)d0.01(1. 02%) f0.00(0.06%)	0.0000 0.0000 0.0000 0.0000 0.0000 0.0000 0.0000 0.9945 0.0085 -0.0031 0.0001 0.0000 0.0000 0.0000 0.0000 0.0000 0.0000 0.0000 0.0000 0.0000

Downloaded from pubs.acs.org/jpcicd/article-supplement/5463676/pdf/jz6c03291_si_001/ by Ralf Kaiser on 23 November 2026

		0.0000 0.0000 0.0000 0.0000 -0.1007 -0.0037 0.0050 0.0000 0.0000 0.0000 0.0000 0.0000 0.0000 0.0000 0.0000 0.0000 0.0000 0.0000 0.0246 0.0006 0.0000 0.0000 0.0000 0.0000 0.0000 0.0000 0.0039 0.0029 0.0000 0.0000
BD(2) S1 - S2 Occupancy 1.99567	33.14% 0.5756* S2 s(0.00%)p1.00(96.63%)d0.03(3. 30%) f0.00(0.07%)	0.0000 0.0000 0.0000 0.0000 0.0000 0.0000 0.0001 0.9807 0.0657 0.0071 0.0150 0.0000 0.0000 0.0000 0.0000 0.0000 0.0000 0.0000 0.0000 0.0000 0.0000 0.0000 0.0000 0.0000 -0.1801 0.0221 -0.0096 0.0000 0.0000 0.0000 0.0000 0.0000 0.0000 0.0000 0.0000 0.0000 0.0000 0.0000 0.0255 -0.0002 0.0000 0.0000 0.0000 0.0000 0.0000 0.0000 -0.0017 0.0046 0.0000 0.0000
BD(1) S2 - O3 Occupancy 1.98812	35.17% 0.5931* S2 s(32.27%)p2.06(66.49%)d0.04(1 .21%) f0.00(0.03%)	-0.0000 -0.0000 0.5670 -0.0346 -0.0023 -0.0004 0.0000 0.0000 0.0000 0.0000 0.0000 0.0000 0.6980 -0.0671 0.0038 0.0028 -0.0000 -0.4145 0.0360 -0.0032 0.0007 0.0000 0.0000 0.0000 0.0000 0.0000 0.0000 0.0889 0.0150 0.0003 0.0501 0.0168 0.0031 0.0345 -0.0041 0.0017 0.0054 0.0014 0.0000 0.0000 0.0067 0.0027 0.0106 0.0002 0.0000 0.0000 0.0000 0.0000 -0.0079 0.0007
BD(1) S2 - O3 Occupancy 1.98812	64.83% 0.8051* O3 s(24.04%)p3.11(74.80%)d0.05(1 .11%) f0.00(0.04%)	0.0000 0.4903 -0.0069 -0.0021 0.0002 0.0000 0.0000 0.0000 0.0000 -0.7449 0.0188 0.0025 0.0008 0.4389 -0.0104 -0.0013 -0.0002 0.0000 0.0000 0.0000 0.0000 0.0000 0.0000 -0.0805 0.0031 -0.0013 -0.0661 0.0054 -0.0004 -0.0150 -0.0014 -0.0005 -0.0102 0.0006 0.0000 0.0000 -0.0026 -0.0001 -0.0154 0.0003 0.0000 0.0000 0.0000 0.0000 0.0096 0.0002
BD(1) S2 - O4 Occupancy 1.98812	35.17% 0.5931* S2 s(32.27%)p2.06(66.49%)d0.04(1 .21%) f0.00(0.03%)	0.0000 0.0000 -0.5670 0.0346 0.0023 0.0004 0.0000 0.0000 0.0000 0.0000 0.0000 0.0000 0.6980 -0.0671 0.0038 0.0028 0.0000 0.4145 -0.0360 0.0032 -0.0007 0.0000 0.0000 0.0000 0.0000 0.0000 0.0000 0.0889 0.0150 0.0003 -0.0501 -0.0168 -0.0031 -0.0345 0.0041 -0.0017 -0.0054 -0.0014 0.0000 0.0000 0.0067 0.0027 -0.0106 -0.0002 0.0000 0.0000 0.0000 0.0000 -0.0079 0.0007
BD(1) S2 - O4 Occupancy 1.98812	64.83% 0.8051* O4 s(24.04%)p3.11(74.80%)d0.05(1 .11%) f0.00(0.04%)	-0.0000 -0.4903 0.0069 0.0021 -0.0002 0.0000 0.0000 0.0000 0.0000 -0.7449 0.0188 0.0025 0.0008 -0.4389 0.0104 0.0013 0.0002 0.0000 0.0000 0.0000 0.0000 0.0000 0.0000 -0.0805 0.0031 -0.0013 0.0661 -0.0054 0.0004 0.0150 0.0014 0.0005 0.0102 -0.0006 0.0000 0.0000 -0.0026 -0.0001 0.0154 -0.0003 0.0000 0.0000 0.0000 0.0000 0.0096 0.0002

Downloaded from pubs.acs.org/jpcicd/article-supplement/5463676/pdf/jz6c03291_si_001/ by Ralf Kaiser on 23 November 2026

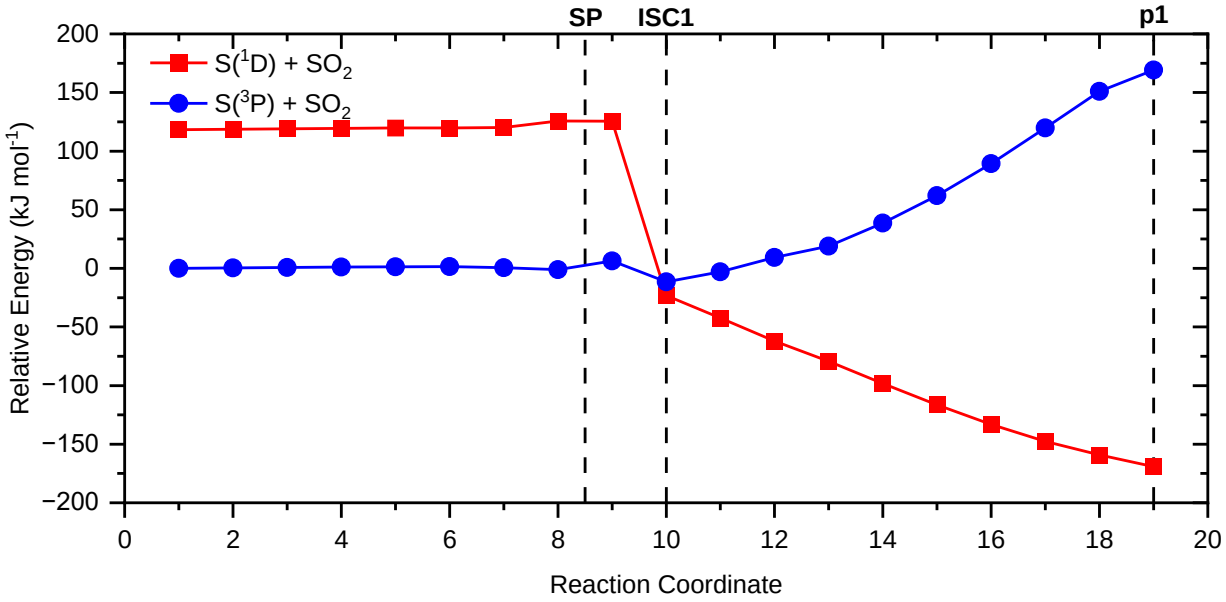

Figure S6. XMS-CASPT2(8,8) energy scan connecting reactants, products, and **ISC1** on the singlet surface (red, CASPT2-1^1A) and the triplet surface (blue, CASPT2-1^3A). Relative energies (in kJ mol^{-1}) are shown for the lowest singlet and triplet states with respect to $S(^3P) + SO_2$. Higher singlet and triplet states included in the XMS-CASPT2 calculations are omitted from the plot for clarity. The reaction coordinate (RC) represents smoothly interpolated structures, where RC = 1 corresponds to the separated reactants, saddle point (SP) lies between RC = 8 and 9, RC = 10 to **ISC1**, and RC = 19 to the singlet SSO_2 product. ZPE corrections are not included.

Downloaded from pubs.acs.org/jpcicd/article-supplement/5463676/pdf/jz6c03291_si_001/ by Ralf Kaiser on 23 November 2026

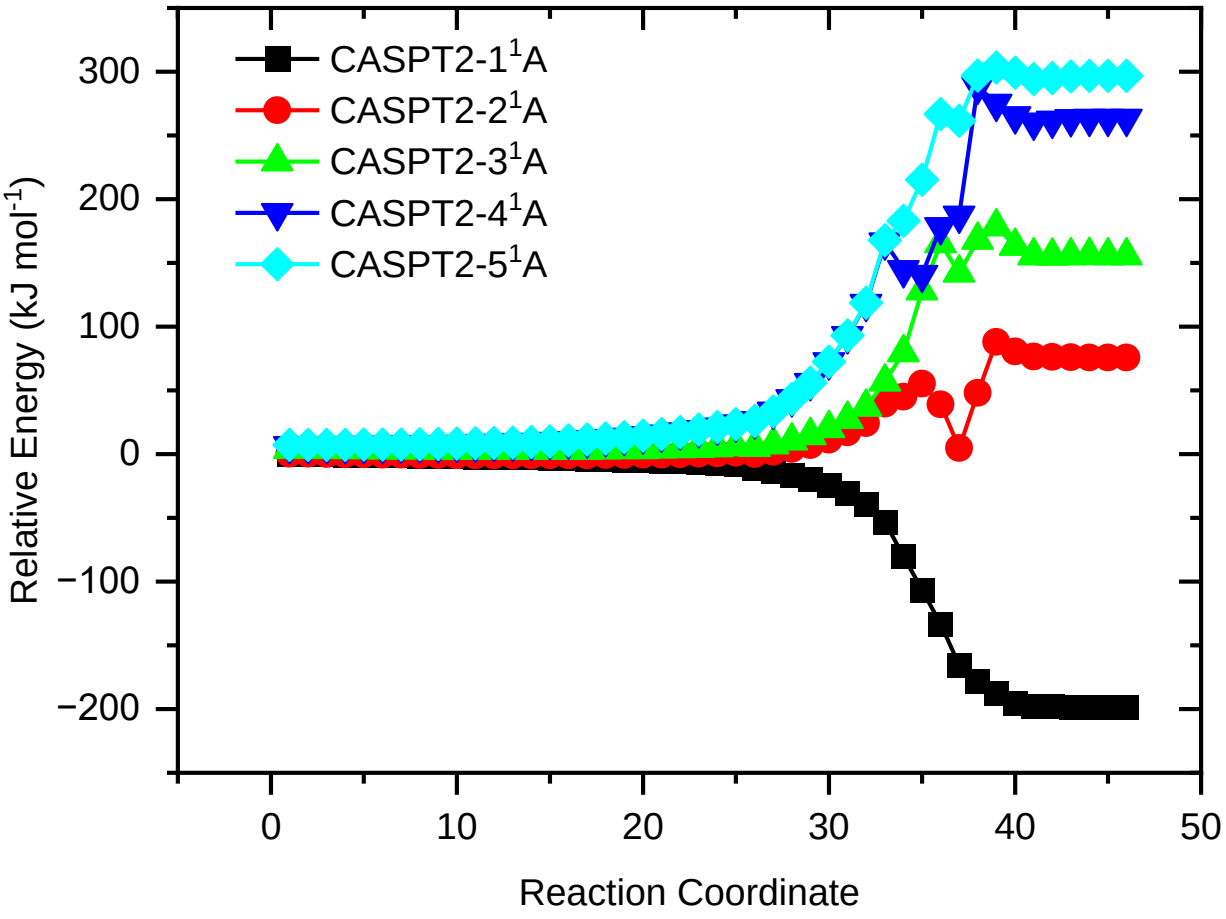

Figure S7. XMS-CASPT2(8,8) energy scan for the addition of S(^{1}D) + SO_2 to form the cyclic intermediate **i1**, including five singlet states to account for the degeneracy of the S(^{1}D) atomic state. Relative energies (in kJ mol^{-1}) are reported with respect to S(^{1}D) + SO_2. The reaction coordinate represents smoothly interpolated structures from the separated reactants to **i1**. ZPE corrections are not included.

Downloaded from pubs.acs.org/jpcicd/article-supplement/5463676/pdf/jz6c03291_si_001/ by Ralf Kaiser on 23 November 2026

Table S9. S_xO_y (x = 1-2, y = 1-4) isomers calculated at the CCSD(T)-F12/cc-pVTZ-F12 level of theory with optimized geometries in Å, energy in hartrees, and harmonic frequencies in cm^{-1}.

SO (3)
SO^+
CCSD(T)-F12/CC-PVTZ-F12 ENERGY=-472.49243151
S 0.0000000000 0.0000000000 -0.4749089858
O 0.0000000000 0.0000000000 0.9516345666
Wavenumbers [cm-1] 1320.92
--
SO (**3**)
CCSD(T)-F12/CC-PVTZ-F12 ENERGY=-472.87093613
S 0.0000000000 0.0000000000 -0.4937614826
O 0.0000000000 0.0000000000 0.9894116738
Wavenumbers [cm-1] 1158.07
--

SO_2 (4)
OSO^+ **4a**$^+$
CCSD(T)-F12/CC-PVTZ-F12 ENERGY=-547.62896794
S 0.0000000000 0.0000000000 -0.2845374843
O 0.0000000000 1.3061369725 0.2850816826
O 0.0000000000 -1.3061369725 0.2850816826
Wavenumbers [cm-1] 612.75 1356.09 1602.86
--
OSO **4a**
CCSD(T)-F12/CC-PVTZ-F12 ENERGY=-548.08285340
S 0.0000000000 0.0000000000 -0.3615519781
O 0.0000000000 1.2367984176 0.3622434722
O 0.0000000000 -1.2367984176 0.3622434722
Wavenumbers [cm-1] 522.91 1175.73 1387.98
--
SOO^+ **4b**$^+$
CCSD(T)-F12/CC-PVTZ-F12 ENERGY=-547.46798134
S 0.0000000000 0.1258921460 -0.9672582958
O 0.0000000000 -0.5661341421 0.4140198442
O 0.0000000000 0.3138682947 1.5241966492
Wavenumbers [cm-1] 342.17 809.48 1968.70
--
SOO **4b**
CCSD(T)-F12/CC-PVTZ-F12 ENERGY=-547.88960103
S 0.0000000000 0.1031246163 -1.0028870773
O 0.0000000000 -0.5052417071 0.4886861674
O 0.0000000000 0.2985980081 1.5209241742
Wavenumbers [cm-1] 479.46 793.82 943.99
--

Downloaded from pubs.acs.org/jpcicd/article-supplement/5463676/pdf/jz6c03291_si_001/ by Ralf Kaiser on 23 November 2026

cyclic-SO_2^+ **4c**$^+$
CCSD(T)-F12/CC-PVTZ-F12 ENERGY=-547.54135441
S 0.0000000000 0.0000000000 -0.6857504947
O 0.0000000000 -0.7914646632 0.6870620417
O 0.0000000000 0.7914646632 0.6870620417
Wavenumbers [cm-1] 604.33 769.40 1036.57
--
cyclic-SO_2 **4c**
CCSD(T)-F12/CC-PVTZ-F12 ENERGY=-547.90512637
S 0.0000000000 0.0000000000 -0.7449575052
O 0.0000000000 -0.7468103111 0.7463822899
O 0.0000000000 0.7468103111 0.7463822899
Wavenumbers [cm-1] 655.13 746.39 966.24
--

SO_3 (5)
dioxathiirane oxide$^+$ **3c**$^+$
CCSD(T)-F12/CC-PVTZ-F12 ENERGY=-622.70861010
O 0.0000000000 0.5486195452 -1.4211455204
S 0.0000000000 -0.4450087370 -0.4337361192
O 0.6673733577 0.1715500755 1.1451384308
O -0.6673733577 0.1715500755 1.1451384308
Wavenumbers [cm-1] 277.50 336.95 456.92 542.81 1141.81
Wavenumbers [cm-1] 1417.32
--
dioxathiirane oxide **3c**
CCSD(T)-F12/CC-PVTZ-F12 ENERGY=-623.11751881
O 0.0000000000 0.4543477383 -1.4186888783
S 0.0000000000 -0.4233440542 -0.2937400459
O 0.7679861787 0.1969798609 1.0036462840
O -0.7679861787 0.1969798609 1.0036462840
Wavenumbers [cm-1] 349.34 464.21 647.30 682.73 958.66
Wavenumbers [cm-1] 1327.38
--
Cyclic$^+$ **3e**$^+$
CCSD(T)-F12/CC-PVTZ-F12 ENERGY=-622.62256520
O 0.0001621454 0.0000000000 -1.2774545899
S 0.0000645728 0.0000000000 0.9332330386
O -0.0001457690 1.0679154813 -0.2962906188
O -0.0001457690 -1.0679154813 -0.2962906188
Wavenumbers [cm-1] 231.44 601.19 762.71 836.60 894.69
Wavenumbers [cm-1] 946.79
--
Cyclic **3e**
CCSD(T)-F12/CC-PVTZ-F12 ENERGY=-622.96635152
O -0.2571627248 0.0000000000 -1.2416611537

Downloaded from pubs.acs.org/jpcicd/article-supplement/5463676/pdf/jz6c03291_si_001/ by Ralf Kaiser on 23 November 2026

S -0.0926066833 0.0000000000 0.9444083506
O 0.2213651627 1.0730577614 -0.3253840225
O 0.2213651627 -1.0730577614 -0.3253840225
Wavenumbers [cm-1] 358.86 608.44 657.03 756.16 762.60
Wavenumbers [cm-1] 837.77
--
D_{3h}^{+} **3a**$^{+}$
CCSD(T)-F12/CC-PVTZ-F12 ENERGY=-622.74410260
O 0.7127400946 1.2345020564 0.0000000000
S -0.0000000000 0.0000000000 0.0000000000
O -1.4254801892 0.0000000000 0.0000000000
O 0.7127400946 -1.2345020564 0.0000000000
Wavenumbers [cm-1] 424.79 1045.65 1081.36 1081.42 23.13 25.99
--
D_{3h} **3a**
CCSD(T)-F12/CC-PVTZ-F12 ENERGY=-623.21954354
O 0.7100494497 1.2298417228 0.0000000000
S 0.0000000000 0.0000000000 0.0000000000
O -1.4200988995 0.0000000000 0.0000000000
O 0.7100494497 -1.2298417228 0.0000000000
Wavenumbers [cm-1] 503.44 533.74 533.85 1086.32 1418.92
Wavenumbers [cm-1] 1418.93
--
OSOO^{+} **3b**$^{+}$
CCSD(T)-F12/CC-PVTZ-F12 ENERGY=-622.69793966
O 0.0000000000 0.3268036553 -1.6825052680
S 0.0000000000 -0.3971658250 -0.4745696235
O 0.0000000000 0.6366210619 0.7628265463
O 0.0000000000 -0.1675738510 1.8706332655
Wavenumbers [cm-1] 122.57 256.54 443.78 788.33 964.97
Wavenumbers [cm-1] 1368.31
--
OSOO **3b**
CCSD-F12/CC-PVTZ-F12 ENERGY=-623.00453586
O 0.0000000000 0.2920763962 -1.7120482615
S 0.0000000000 -0.3730444146 -0.4564315411
O 0.0000000000 0.5906912296 0.7082089119
O 0.0000000000 -0.1352518483 1.9184483479
Wavenumbers [cm-1] 141.37 157.75 475.31 642.38 987.69
Wavenumbers [cm-1] 1363.20
--
SOOO^{+} **3d**$^{+}$
CCSD(T)-F12/CC-PVTZ-F12 ENERGY=-622.49268852
S 0.0000000000 0.0006028166 -1.3484058675
O 0.0000000000 0.0001669162 0.5003039628
O 0.0000000000 1.1198909883 1.1021976262

Downloaded from pubs.acs.org/jpcicd/article-supplement/5463676/pdf/jz6c03291_si_001/ by Ralf Kaiser on 23 November 2026

O 0.0000000000 -1.1212658437 1.0994679919
Wavenumbers [cm-1] 220.15 316.95 419.55 699.84 940.86
Wavenumbers [cm-1] 1049.35
--
SOOO **3d**
CCSD(T)-F12/CC-PVTZ-F12 ENERGY=-622.87439230
S 0.0000000000 0.0000317383 -1.2816278450
O 0.0000000000 0.0000539167 0.4059546326
O 0.0000000000 1.1276442497 1.0811844979
O 0.0000000000 -1.1277617644 1.0810189697
Wavenumbers [cm-1] 392.15 418.76 522.43 700.79 911.77
Wavenumbers [cm-1] 917.31
--

S_2O (6)
SSO^+ **6a$^+$, 6c$^+$**
CCSD(T)-F12/CC-PVTZ-F12 ENERGY=-870.28038705
S 0.0000000000 0.1552342146 -1.3186178166
S 0.0000000000 -0.4609207471 0.5617469889
O 0.0000000000 0.6125423598 1.5166367950
Wavenumbers [cm-1] 236.36 531.89 1237.67
--
SSO **6a**
CCSD(T)-F12/CC-PVTZ-F12 ENERGY=-870.66985189
S 0.0000000000 0.1649705888 -1.2832352959
S 0.0000000000 -0.4427305195 0.5028755622
O 0.0000000000 0.5565823331 1.5637044552
Wavenumbers [cm-1] 384.91 695.92 1193.91
--
SOS^+ **6b$^+$**
CCSD(T)-F12/CC-PVTZ-F12 ENERGY=-870.21207754
S 0.0000000000 0.1841996078 -1.3281589672
O 0.0000000000 -0.7381304750 -0.0001110809
S 0.0000000000 0.1841611134 1.3282144016
Wavenumbers [cm-1] 304.75 791.91 891.23
--
SOS **6b**
CCSD(T)-F12/CC-PVTZ-F12 ENERGY=-870.56591237
S 0.0000000000 -1.4449845295 0.1480347823
O 0.0000000000 0.0000000000 -0.5932716379
S 0.0000000000 1.4449845295 0.1480347823
Wavenumbers [cm-1] 335.58 684.16 808.14
--
Cyclic **6c**
CCSD(T)-F12/CC-PVTZ-F12 ENERGY=-870.59762747

Downloaded from pubs.acs.org/jpcicd/article-supplement/5463676/pdf/jz6c03291_si_001/ by Ralf Kaiser on 23 November 2026

S 0.0000000000 -1.0154050348 -0.2749172856
O 0.0000000000 0.0000000000 1.1017723385
S 0.0000000000 1.0154050348 -0.2749172856
Wavenumbers [cm-1] 554.45 588.67 815.90

SO_4
Tetrahedral$^+$ **2a$^+$**
CCSD(T)-F12/CC-PVTZ-F12 ENERGY=-697.81603443
S 0.0000000000 0.0000000000 -0.3319948988
O 0.0000000000 1.2802978952 -0.8866625446
O 0.0000000000 -1.2802978952 -0.8866625446
O -0.7014020330 0.0000000000 1.2192924075
O 0.7014020330 0.0000000000 1.2192924075
Wavenumbers [cm-1] 312.18 396.03 429.25 436.88 443.93
Wavenumbers [cm-1] 670.03 1029.60 1261.28 1564.27
--
Tetrahedral **2a**
CCSD(T)-F12/CC-PVTZ-F12 ENERGY=-698.26730398
O -0.8032558113 0.0000043691 -1.1316153299
S -0.0002201164 -0.0000000013 0.2238156358
O 0.0001494135 1.2345296218 0.9073734563
O 0.0001444803 -1.2345307763 0.9073715466
O 0.8034029924 -0.0000032120 -1.1316170715
Wavenumbers [cm-1] 317.59 492.32 494.66 507.63 637.04
Wavenumbers [cm-1] 784.72 952.65 1298.11 1470.21
--
C_2-$O_2SO_2^+$ **2b$^+$**
CCSD(T)-F12/CC-PVTZ-F12 ENERGY=-697.71978715
S 0.0000000000 -0.0000000000 -0.5718701780
O -0.7312322712 1.2109692779 0.2867356693
O 0.7312322712 -1.2109692779 0.2867356693
O 0.7301299764 1.2127975072 0.2862282514
O -0.7301299764 -1.2127975072 0.2862282514
Wavenumbers [cm-1] 349.34 464.57 733.96 786.16 874.86
Wavenumbers [cm-1] 1032.97 1115.82 1538.15 2217.83
--
C_2-O_2SO_2 **2b**
CCSD(T)-F12/CC-PVTZ-F12 ENERGY=-698.13876324
S 0.0000000000 -0.0000000000 -0.4792006059
O -0.8555668268 0.9724978206 0.4156367785
O 0.8555668268 -0.9724978206 0.4156367785
O 0.5579340341 1.4912818068 0.0644803329

Downloaded from pubs.acs.org/jpcicd/article-supplement/5463676/pdf/jz6c03291_si_001/ by Ralf Kaiser on 23 November 2026

O -0.5579340341 -1.4912818068 0.0644803329
Wavenumbers [cm-1] 250.69 349.79 435.41 552.28 613.03
Wavenumbers [cm-1] 740.43 749.95 962.21 1040.06
--

Downloaded from pubs.acs.org/jpcicd/article-supplement/5463676/pdf/jz6c03291_si_001/ by Ralf Kaiser on 23 November 2026

Table S10. Geometries, energies, and frequencies of computed molecules. Optimized Cartesian coordinates (Å), XMS-CASPT2(8,8)/def2-TZVPPD electronic energies (Hartree), zero-point energies (Hartree), and vibrational frequencies (cm^{-1}) at the ωB97X-D4/def2-TZVPPD level.

========== SO_2 ==========

Singlet state
ZPE: 0.00731986
Vibrational Frequencies:
535.90 1238.55 1438.59
Atomic Coordinates:

S	-2.00113266750199	0.87305919616545	0.00000000000000
O	-0.73895247750975	1.54342971076032	0.00000000000000
O	-3.20049116758826	1.65026138147423	0.00000000000000

========== S + SO_2 ==========

Note: The separation between S and SO_2 is 10 Å.

Singlet state
Energy: -945.53884214

Triplet state
Energy: -945.58394230

========== IM1 ==========

Singlet state
Energy: -945.61505913
ZPE: 0.00920136
Vibrational Frequencies:
292.87 434.13 495.75
619.73 877.21 1319.24
Atomic Coordinates:

S	-0.04947221740977	-0.30776910603844	-1.14562623735980
S	0.55203757481595	0.19348157297479	0.76372975440752
O	-0.22067879187361	1.22560000809781	1.39242503693397
O	-0.33806504165754	-1.11068249763034	0.37769813245438

========== TS1 ==========

Triplet state
Energy: -945.58144831
ZPE: 0.00780124
Vibrational Frequencies:
67.66 167.44 530.45
1228.19 1430.61
Atomic Coordinates:

S	0.00778801374431	-0.06165634498234	-2.12639840554500
S	-0.00218272805959	0.30124333682908	0.59593045896099

Downloaded from pubs.acs.org/jpcicd/article-supplement/5463676/pdf/jz6c03291_si_001/ by Ralf Kaiser on 23 November 2026

O	1.23290339116532	-0.22269568108374	1.08762828684824
O	-1.23729867685004	-0.22786831076300	1.08199165973577

========== Saddle Point ==========

Singlet state
Energy: -945.54004623
ZPE: 0.00754888
Vibrational Frequencies:
62.07 68.18 523.63
1222.64 1437.05
Atomic Coordinates:

S	-0.08194775493981	0.00006607413336	-2.28469460582395
S	0.43030063067280	-0.00004123676883	0.97780617116439
O	-0.17418673950775	1.23093462971893	1.38085702513564
O	-0.17416613622524	-1.23095946708347	1.38106039652392

========== TS2 ==========

Singlet state
Energy: -945.54909484
ZPE: 0.00821301
Vibrational Frequencies:
266.35 383.95 486.26
1091.85 1376.68
Atomic Coordinates:

S	0.42232224481867	0.30550691232784	-1.33537697611554
S	0.39169072428289	0.18070491685564	0.73614417464592
O	-0.18739601563057	1.21263388759478	1.53509034944408
O	-0.29798095347099	-1.08325471677826	0.48133945202554

========== SSO_2 ==========

Singlet state
Energy: -945.64043139
ZPE: 0.01064362
Vibrational Frequencies:
361.36 430.02 490.55
715.69 1238.94 1435.46
Atomic Coordinates:

S	-0.00000007891697	-0.00000075579089	-1.47894095788082
S	0.00000028212666	0.00000050323873	0.37998328625007
O	-0.00000010160511	1.22992511974523	1.09894012691850
O	-0.00000010160459	-1.22992486719307	1.09893883861226

Triplet state
Energy: -945.58647068
ZPE: 0.00892725
Vibrational Frequencies:

Downloaded from pubs.acs.org/jpcicd/article-supplement/5463676/pdf/jz6c03291_si_001/ by Ralf Kaiser on 23 November 2026

152.60 300.88 456.07
510.77 1144.99 1353.31
Atomic Coordinates:

S	0.00000682882475	-0.05583989553392	-1.53620390120163
S	-0.00000270978820	0.27068403160394	0.52521297135107
O	1.26230686512195	-0.21291069688035	1.02506464727299
O	-1.26231098415850	-0.21291050958967	1.02507755487756

========== ISC1 ==========
Singlet state
Energy: -945.59270148
Triplet state
Energy: -945.58828711
Mean: -945.59049430
ZPE: 0.00749908
Vibrational Frequencies:
157.47 221.42 477.42
1049.03 1386.39
Atomic Coordinates:

S	0.0000000000	-0.0489917737	-1.5748746711
S	0.0000000000	0.2421680301	0.5224860322
O	1.2273795985	-0.1935457199	1.0544014077
O	-1.2273795985	-0.1935457199	1.0544014077

Downloaded from pubs.acs.org/jpcicd/article-supplement/5463676/pdf/jz6c03291_si_001/ by Ralf Kaiser on 23 November 2026

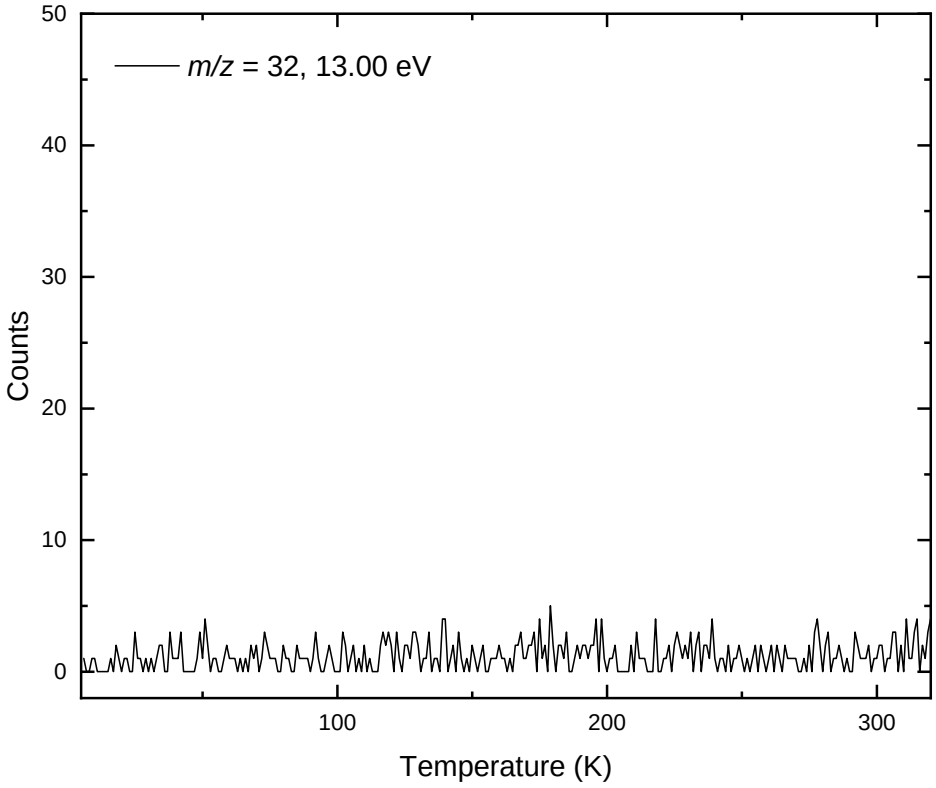

Figure S8. TPD profile of *m/z* = 32 at 13.00 eV in irradiated SO_2 ices using synchrotron vacuum ultraviolet photoionization reflectron time-of-flight mass spectrometry.

Downloaded from pubs.acs.org/jpcicd/article-supplement/5463676/pdf/jz6c03291_si_001/ by Ralf Kaiser on 23 November 2026

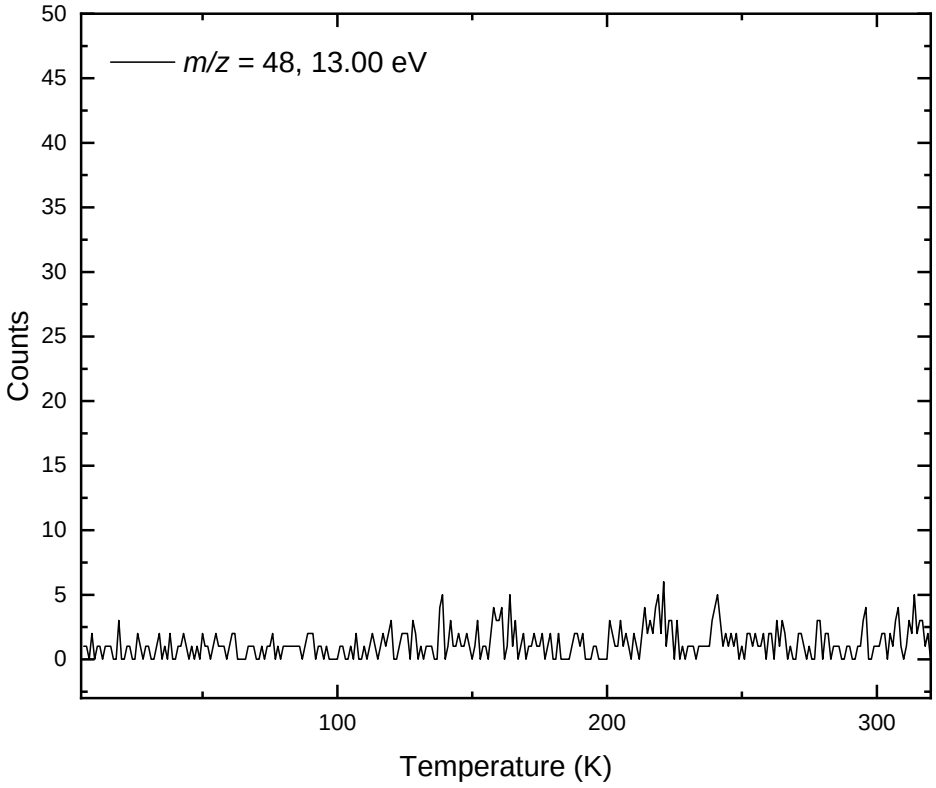

Figure S9. TPD profile of *m/z* = 48 at 13.00 eV in irradiated SO_2 ices using synchrotron vacuum ultraviolet photoionization reflectron time-of-flight mass spectrometry.

Downloaded from pubs.acs.org/jpcicd/article-supplement/5463676/pdf/jz6c03291_si_001/ by Ralf Kaiser on 23 November 2026

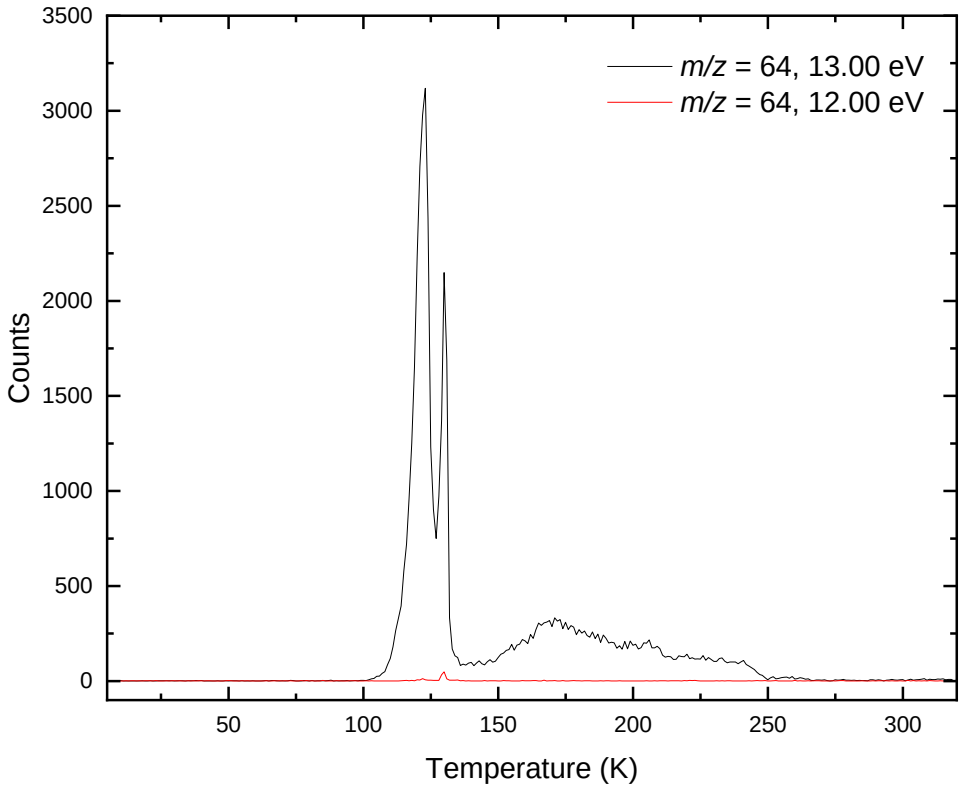

Figure S10. TPD profile of *m/z* = 64 at 13.00 eV (black) and 12.00 eV (red) in irradiated SO_2 ices using synchrotron vacuum ultraviolet photoionization reflectron time-of-flight mass spectrometry.

Downloaded from pubs.acs.org/jpcicd/article-supplement/5463676/pdf/jz6c03291_si_001/ by Ralf Kaiser on 23 November 2026

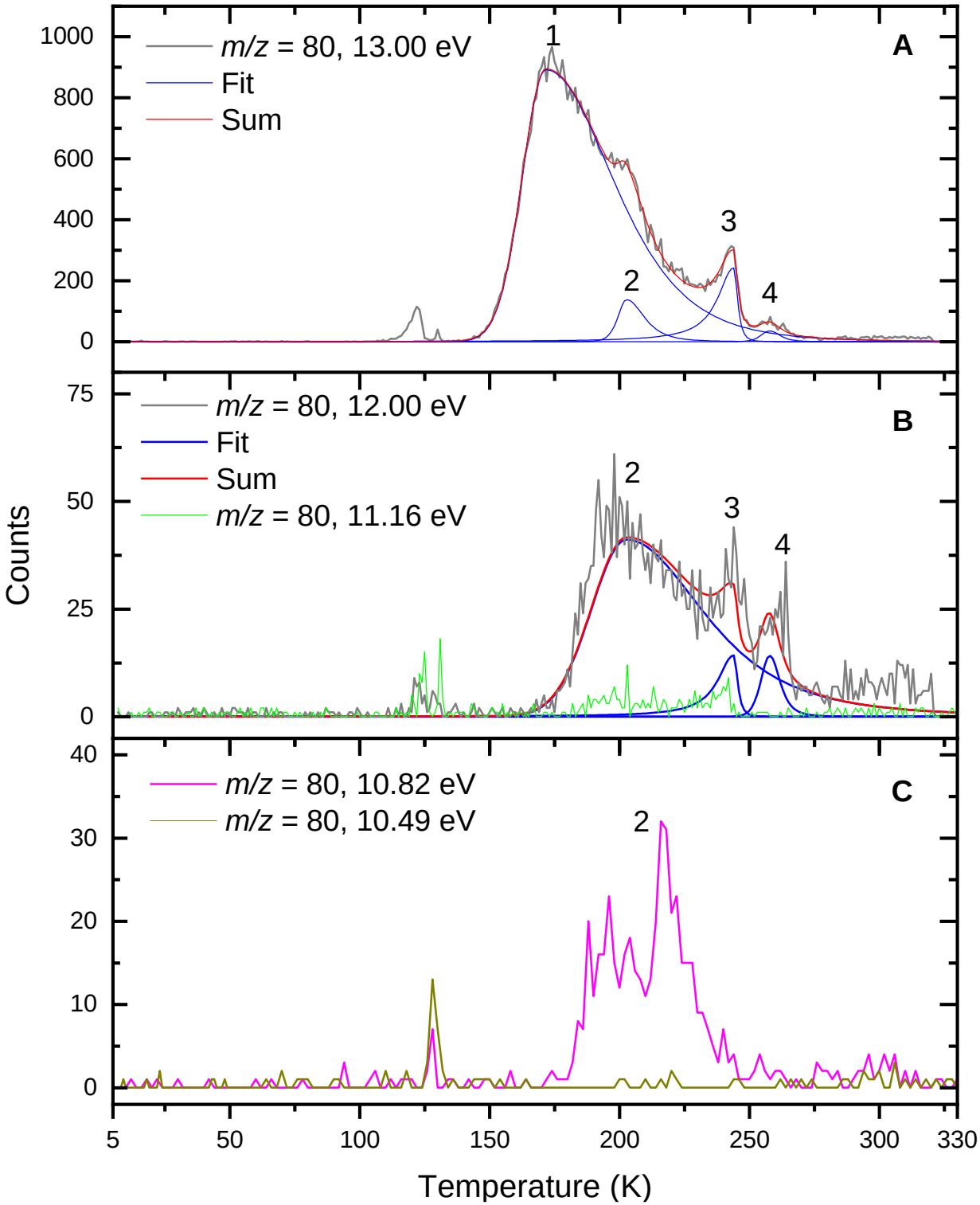

Figure S11. TPD profiles measured at 13.00 eV (**A**), 12.00 eV with 11.16 eV (**B**), and 10.82 eV with 10.49 eV (**C**) of pure SO_2 ices. The profiles were deconvoluted (blue) and summed (red) to untangle sublimation events from one another labeled as **1-4**.

Downloaded from pubs.acs.org/jpcicd/article-supplement/5463676/pdf/jz6c03291_si_001/ by Ralf Kaiser on 23 November 2026

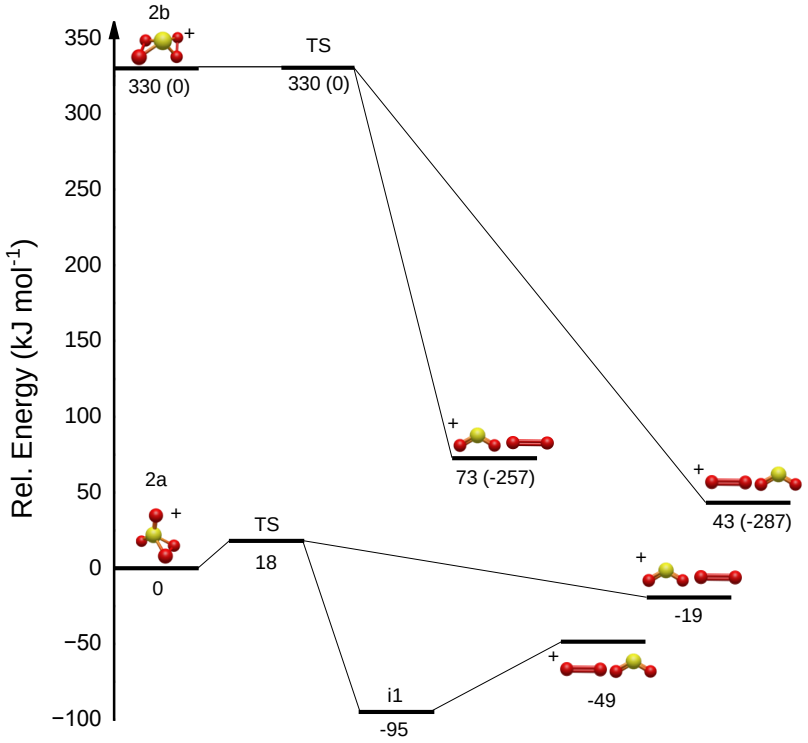

Figure S12. Decomposition of SO_4^+ towards O_2 and SO_2 calculated at the CCSD(T)-F12/cc-pVTZ-F12 (F12-TZ) level of theory. Each isomer (**2a** and **2b**) shows decomposition towards $SO_2 + O_2^+$ and $SO_2^+ + O_2$.

Downloaded from pubs.acs.org/jpcicd/article-supplement/5463676/pdf/jz6c03291_si_001/ by Ralf Kaiser on 23 November 2026

REFERENCES

1. Yarnall, Y. Y.; Hudson, R. L., A New Method for Measuring Infrared Band Strengths in H_2O Ices: First Results for OCS, H_2S, and SO_2. *Astrophys. J. Lett.* **2022**, *931*, L4.
2. Wang, J.; Marks, J. H.; Turner, A. M.; Nikolayev, A. A.; Azyazov, V.; Mebel, A. M.; Kaiser, R. I., Mechanistical study on the formation of hydroxyacetone (CH_3COCH_2OH), methyl acetate (CH_3COOCH_3), and 3-hydroxypropanal ($HCOCH_2CH_2OH$) along with their enol tautomers (prop-1-ene-1,2-diol ($CH_3C(OH)CHOH$), prop-2-ene-1,2-diol ($CH_2C(OH)CH_2OH$), 1-methoxyethen-1-ol ($CH_3OC(OH)CH_2$) and prop-1-ene-1,3-diol ($HOCH_2CHCHOH$)) in interstellar ice analogs. *Phys. Chem. Chem. Phys.* **2023**, *25*, 936-953.
3. Bergantini, A.; Góbi, S.; Abplanalp, M. J.; Kaiser, R. I., A Mechanistical Study on the Formation of Dimethyl Ether (CH_3OCH_3) and Ethanol (CH_3CH_2OH) in Methanol-containing Ices and Implications for the Chemistry of Star-forming Regions. *Astrophys. J.* **2018**, *852*, 70.
4. Bennett, C. J.; Jamieson, C.; Mebel, A. M.; Kaiser, R. I., Untangling the formation of the cyclic carbon trioxide isomer in low temperature carbon dioxide ices. *Phys. Chem. Chem. Phys.* **2004**, *6*, 735-746.
5. Bennett, C. J.; Jamieson, C. S.; Osamura, Y.; Kaiser, R. I., Laboratory studies on the irradiation of methane in interstellar, cometary, and solar system ices. *Astrophys. J.* **2006**, *653*, 792.
6. Drouin, D.; Couture, A. R.; Joly, D.; Tastet, X.; Aimez, V.; Gauvin, R., CASINO V2.42: a fast and easy-to-use modeling tool for scanning electron microscopy and microanalysis users. *Scanning* **2007**, *29*, 92-101.
7. Adler, T. B.; Knizia, G.; Werner, H. J., A simple and efficient CCSD(T)-F12 approximation. *J. Chem. Phys.* **2007**, *127*, 221106.
8. Knizia, G.; Adler, T. B.; Werner, H. J., Simplified CCSD(T)-F12 methods: theory and benchmarks. *J. Chem. Phys.* **2009**, *130*, 054104.
9. Peterson, K. A.; Adler, T. B.; Werner, H.-J., Systematically convergent basis sets for explicitly correlated wavefunctions: The atoms H, He, B–Ne, and Al–Ar. *J. Chem. Phys.* **2008**, *128*.
10. Werner, H. J., et al., MOLPRO, version 2025.1, a package of ab initio programs. **2025**.
11. Werner, H.-J.; Knowles, P. J.; Knizia, G.; Manby, F. R.; Schütz, M., Molpro: a general-purpose quantum chemistry program package. *WIREs Comput. Mol. Sci.* **2012**, *2*, 242-253.
12. Wang, J.; Turner, A. M.; Marks, J. H.; Fortenberry, R. C.; Kaiser, R. I., Formation of Paraldehyde ($C_6H_{12}O_3$) in Interstellar Analog Ices of Acetaldehyde Exposed to Ionizing Radiation. *ChemPhysChem* **2024**, *25*, e202400837.
13. Wang, J.; Turner, A. M.; Marks, J. H.; Zhang, C.; Kleimeier, N. F.; Bergantini, A.; Singh, S. K.; Fortenberry, R. C.; Kaiser, R. I., Preparation of Acetylenediol (HOCCOH) and Glyoxal (HCOCHO) in Interstellar Analog Ices of Carbon Monoxide and Water. *Astrophys. J.* **2024**, *967*, 79.
14. Becke, A. D., Density-Functional Thermochemistry. III. The Role of Exact Exchange. *J. Chem. Phys.* **1993**, *98*, 5648-5652.
15. Dunning, T. H., Gaussian Basis Sets for Use in Correlated Molecular Calculations. I. The Atoms Boron through Neon and Hydrogen. *J. Chem. Phys.* **1989**, *90*, 1007-1023.
16. Dunning, T. H.; Peterson, K. A.; Wilson, A. K., Gaussian Basis Sets for Use in Correlated Molecular Calculations. X. The Atoms Aluminum Through Argon Revisited. *J. Chem. Phys.* **2001**, *114*, 9244-9253.

Downloaded from pubs.acs.org/jpcld/article-supplement/5463676/pdf/jz6c03291_si_001/ by Ralf Kaiser on 23 November 2026

17. Lee, C. T.; Yang, W. T.; Parr, R. G., Development of the Colle-Salvetti Correlation-Energy Formula into a Functional of the Electron Density. *Phys. Rev. B* **1988**, *37*, 785-789.
18. Yang, W. T.; Parr, R. G.; Lee, C. T., Various Functionals for the Kinetic Energy Density of an Atom or Molecule. *Phys. Rev. A* **1986**, *34*, 4586-4590.
19. Glendening, E.; Reed, A.; Carpenter, J.; Weinhold, F., NBO Version 3.1. *TCI, University of Wisconsin, Madison* **1998**, *65*.
20. Weinhold, F.; Carpenter, J. E., In *The Structure of Small Molecules and Ions*, Naaman, R.; Vager, Z., Eds. Plenum: 1988; pp 227-236.
21. Frisch, M. J., et al. *Gaussian 16 Revision C.01*, Gaussian Inc.: Wallingford, CT, 2016.
22. Neese, F., The ORCA program system. *WIREs Comput. Mol. Sci.* **2012**, *2*, 73-78.
23. Neese, F., Software update: The ORCA program system—Version 6.0. *WIREs Comput. Mol. Sci.* **2025**, *15*, e70019.
24. Chai, J.-D.; Head-Gordon, M., Systematic optimization of long-range corrected hybrid density functionals. *J. Chem. Phys.* **2008**, *128*, 084106.
25. Caldeweyher, E.; Mewes, J.-M.; Ehlert, S.; Grimme, S., Extension and evaluation of the D4 London-dispersion model for periodic systems. *Phys. Chem. Chem. Phys.* **2020**, *22*, 8499-8512.
26. Weigend, F.; Ahlrichs, R., Balanced basis sets of split valence, triple zeta valence and quadruple zeta valence quality for H to Rn: Design and assessment of accuracy. *Phys. Chem. Chem. Phys.* **2005**, *7*, 3297.
27. Fukui, K., Formulation of the reaction coordinate. *J. Phys. Chem.* **1970**, *74*, 4161-4163.
28. Ischtwan, J.; Collins, M. A., Determination of the intrinsic reaction coordinate: Comparison of gradient and local quadratic approximation methods. *J. Chem. Phys.* **1988**, *89*, 2881-2885.
29. Maeda, S.; Harabuchi, Y.; Ono, Y.; Taketsugu, T.; Morokuma, K., Intrinsic reaction coordinate: Calculation, bifurcation, and automated search. *International Journal of Quantum Chemistry* **2015**, *115*, 258-269.
30. Roos, B. O.; Taylor, P. R.; Siegbahn, P. E. M., A complete active space SCF method (CASSCF) using a density matrix formulated super-CI approach. *Chem. Phys.* **1980**, *48*, 157-173.
31. Werner, H.-J., et al., The Molpro quantum chemistry package. *J. Chem. Phys.* **2020**, *152*, 144107.
32. Koga, N.; Morokuma, K., Determination of the lowest energy point on the crossing seam between two potential surfaces using the energy gradient. *Chem. Phys. Lett.* **1985**, *119*, 371-374.
33. Busch, T.; Esposti, A. D.; Werner, H.-J., Analytical energy gradients for multiconfiguration self-consistent field wave functions with frozen core orbitals. *J. Chem. Phys.* **1991**, *94*, 6708-6715.
34. Yang, Z.; Doddipatla, S.; He, C.; Goettl, S. J.; Kaiser, R. I.; Jasper, A. W.; Gomes, A. C. R.; Galvão, B. R. L., Can third-body stabilisation of bimolecular collision complexes in cold molecular clouds happen? *Molecular Physics* **2024**, *122*, e2134832.
35. Harvey, J. N.; Aschi, M., Spin-forbidden dehydrogenation of methoxy cation: A statistical view. *Phys. Chem. Chem. Phys.* **1999**, *1*, 5555-5563.
36. Celani, P.; Werner, H.-J., Multireference perturbation theory for large restricted and selected active space reference wave functions. *J. Chem. Phys.* **2000**, *112*, 5546-5557.

Downloaded from pubs.acs.org/jpcicd/article-supplement/5463676/pdf/jz6c03291_si_001/ by Ralf Kaiser on 23 November 2026

37. Shiozaki, T.; Győrffy, W.; Celani, P.; Werner, H.-J., Communication: Extended multi-state complete active space second-order perturbation theory: Energy and nuclear gradients. *J. Chem. Phys.* **2011**, *135*, 081106.
38. Győrffy, W.; Shiozaki, T.; Knizia, G.; Werner, H.-J., Analytical energy gradients for second-order multireference perturbation theory using density fitting. *J. Chem. Phys.* **2013**, *138*, 104104.
39. Roos, B. O.; Andersson, K., Multiconfigurational perturbation theory with level shift — the Cr2 potential revisited. *Chem. Phys. Lett.* **1995**, *245*, 215-223.
40. Moore, M. H., Studies of proton-irradiated SO_2 at low temperatures: Implications for Io. *Icarus* **1984**, *59*, 114-128.
41. Baran, E. J.; Aymonino, P. J., The I.R. spectra of silver and thallium (I) sulphates. *Spectrochim. Acta, Part A* **1968**, *24*, 288-291.
42. Garozzo, M.; Fulvio, D.; Gomis, O.; Palumbo, M. E.; Strazzulla, G., H-implantation in SO_2 and CO_2 ices. *Planet. Space Sci.* **2008**, *56*, 1300-1308.
43. McAnally, M.; Bocková, J.; Herath, A.; Turner, A. M.; Meinert, C.; Kaiser, R. I., Abiotic formation of alkylsulfonic acids in interstellar analog ices and implications for their detection on Ryugu. *Nat. Commun.* **2024**, *15*, 4409.
44. Tonkyn, R. G.; Winniczek, J. W.; White, M. G., Rotationally resolved photoionization of O_2^+ near threshold. *Chem. Phys. Lett.* **1989**, *164*, 137-142.
45. Probst, M.; Hermansson, K.; Urban, J.; Mach, P.; Muigg, D.; Denifl, G.; Fiegele, T.; Mason, N. J.; Stamatovic, A.; Märk, T. D., Ionization energy studies for ozone and OClO monomers and dimers. *The Journal of Chemical Physics* **2002**, *116*, 984-992.
46. Lias, S. G.; Bartmess, J. E.; Liebman, J. F.; Holmes, J. L.; Levin, R. D.; Mallard, W. G., Ion Energetics Data. In *NIST Chemistry WebBook, NIST Standard Reference Database Number 69*, Linstrom, P. J.; Mallard, W. G., Eds. National Institute of Standards and Technology: Gaithersburg, MD.
47. Socrates, G., *Infrared and Raman Characteristic Group Frequencies*, 3rd ed.: Wiley, 2004.

Downloaded from pubs.acs.org/jpcicd/article-supplement/5463676/pdf/jz6c03291_si_001/ by Ralf Kaiser on 23 November 2026